© 2008 ASM International. All Rights Reserved.

Overview of the Mechanisms of Failure in Heat Treated Steel Components

Scott MacKenzie, Houghton International, Inc.

"Primum non nocere" — "First do no harm," attributed to the ancient Roman physician Galen. "Declare the past, diagnose the present, foretell the future; practice these acts . . . make a habit of two things — to help, or at least to do no harm" (Ref 1).

FAILURES IN STEEL components, like any other material, may have various consequences, such as:

- Making the device or component completely inoperable
- Preventing an operable device from functioning satisfactorily
- Making the device or component unsafe or unreliable, with immediate removal from service required

Many aspects may also be involved in tracing back to the possible sources of failure of a component. Some of these sources include:

- Design
- Material issues, such as improper materials selection or material imperfections (laps, seams, inclusions, porosity, etc.)
- Fabrication and processing
- Rework
- Assembly
- Inspection
- Storage and shipment
- Service conditions
- Maintenance
- Unanticipated service conditions

Many times, more than one factor contributes to a part failure. Rarely is it only one factor.

General Sources of Failure

Design deficiencies are a common source of component failure. Examples include the presence of a sharp notch in regions of high stress or a fillet radii that is too sharp. Using a component design for a new application can also lead to unanticipated failures. Higher stresses or unanticipated service conditions can cause unforeseen failure because of complex or increased stress fields. Stress concentrations may become more critical because of the increase in loading for the new application.

Insufficient design criteria can also be the cause of unforeseen failures. Inadequate knowledge of the stress state in the component or inadequate stress calculations can contribute to failures. Much higher stress states than initially assumed or improper stress assumptions can result in premature service failures. Lack of consideration of severe environmental, fatigue, or impact conditions may contribute to failure.

Material issues can usually be attributed to either selection of material or material imperfections rendering it unsuitable for service. Inadequate material data can also result in conditions that may contribute to failure. For example, adequate fatigue data, elevated-temperature tensile data, or creep or corrosion data may not be available, and the designer may have to extrapolate or estimate the effects or these properties.

Other sources of failure can be attributed to material imperfections. For wrought products, this could be related to segregation, inclusions, porosity, laps, and seams. For castings, these imperfections could be cold shuts, inclusions, shrinkage, voids, and porosity. Forgings can have laps, seams, segregation, and anisotropy in properties from forging flow lines.

In one example (Fig. 1), a large roll was heat treated, and several large cracks were observed after inspection. This was originally attributed to quench cracking. On further examination, it was determined that a lap was present in the forging,

© 2008 ASM International. All Rights Reserved.

indicated by the presence of high-temperature oxides in the crack along the crack faces.

Manufacture and Processing. Processing can have a large influence on properties and the resulting residual stresses. Typically, this is related to wrong procedures or improperly specified procedures. Ambiguous processes or specifications can also contribute to failures due to interpretation or application. Simple things like improper selection of processing sequences or procedures or specifications that were not followed can also contribute to failure.

Cold forming, such as stretching or deep drawing, can develop highly localized residual stresses. Local changes in microstructure can occur. Because of the changes in reduction, a large anisotropy in material properties also results. Due to the drawing operation, cracks or microcracking can occur. This could be due to improper lubrication or improper die design. The localized changes in ductility can also contribute to failure.

Machining and grinding can create high residual stresses from either machining practice (feeds and speeds) or improper cutting tool selection, material, or geometry. Grinding, if abusive, can cause large temperature gradients and localized overheating. This overheating can cause changes in microstructure—either localized softening of the material or localized transformation to martensite and other transformation products—resulting in hard spots.

In Fig. 2, a large gear was ground after heat treatment. Because of abusive grinding, local temperatures exceeded the austenitization temperature, and transformation to martensite occurred upon cooling. This transformation and the resulting residual stresses caused cracking of the gear. Temper etch examination of the gear using dilute nitric acid in water in the regions of cracking showed evidence of localized abusive grinding.

Identification of parts can also cause failure to initiate. This is from localized impact or electroetching. Localized mechanical stress concentrations or changes in microstructure can occur. This creates either a mechanical or microstructural notch or stress concentration.

Heat treatment can cause a variety of different root causes for failures. Overheating, decarburization, quenching, tempering, annealing, and other heat treatments can cause failure to occur.

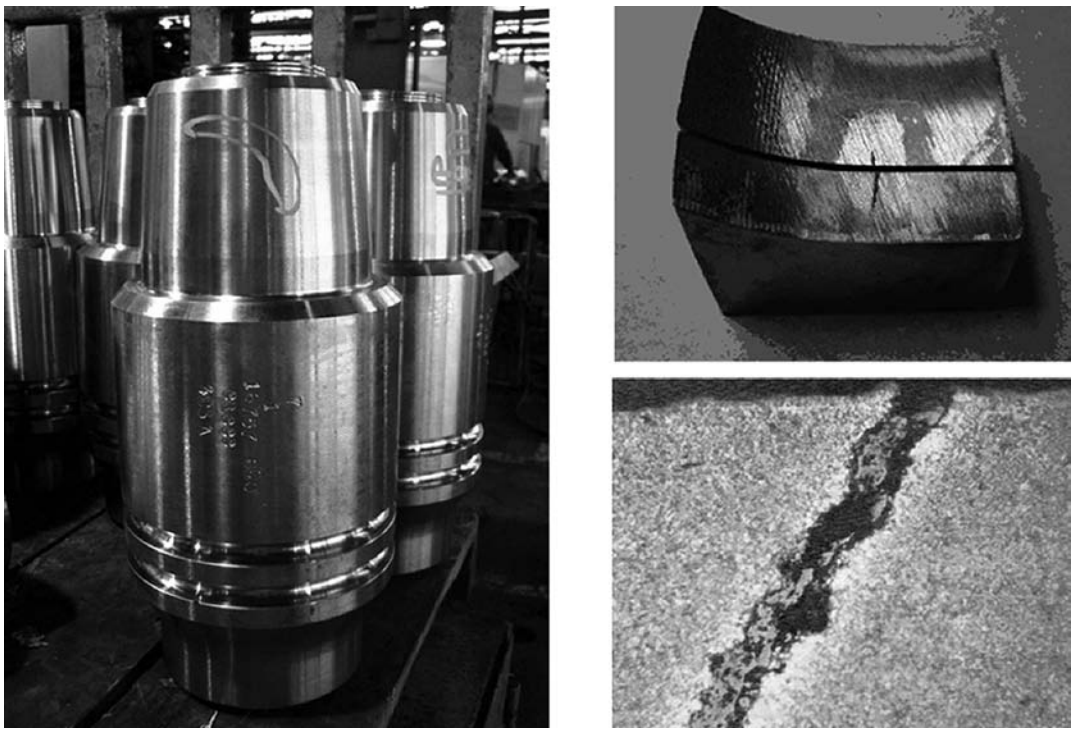

Fig. 1 A large roll was found to have cracks on the outer and inner surfaces of the forging. These cracks were found during final inspection. During examination of metallographic sections taken from the roll, high-temperature oxides were found on the crack faces, strongly suggesting forging laps.

© 2008 ASM International. All Rights Reserved.
Failure Analysis of Heat Treated Steel Component (#05113G) www.asminternational.org

This could also include improper austenitization temperatures and times. Decarburization is the result of a low-carbon surface from improper atmosphere control. Typically, there is a depleted carbon layer at the surface that, when quenched, is softer than the core material. This soft layer can be completely devoid of carbon (complete decarburization) or only partially depleted in carbon (partial decarburization). This decarburized layer can contribute to premature fatigue failures, because the surface material is different than the designer expected, or failure can result from high residual stresses created at the surface from the quenching operation. The low-carbon surface area can also result in distortion—again, high residual tensile stresses at the surface with low surface hardness. Carburization is similar to the effects of decarburization. In this case, there is a higher surface carbon than expected. High residual tensile stresses can result as well as increased distortion.

Quenching can also contribute to high residual stresses or the formation of cracks or microcracking. Transformation stresses from quenching cause the high residual stresses. These high residual tensile stresses can drastically reduce the fatigue strength or have other ramifications in service.

Overheating can cause excessive grain growth, with resulting increases in hardenability and increased embrittlement. Underheating can cause poor mechanical properties, because there was an incomplete transformation to austenite and therefore an incomplete transformation to martensite. Poor mechanical properties, such as low tensile and yield stress, and poor impact properties may occur.

There are also several embrittlement mechanisms caused by the use of improper tempering temperatures. Temper embrittlement and blue brittleness are just two of the common mechanisms that can occur from improper heat treatment and tempering operations.

Cleaning, pickling, and electroplating operations can also cause potential failures or contribute to them. Hydrogen charging of high-strength steels from the dissociation of hydrogen on the surface of high-strength steel can occur from cleaning operations in acids. Charging of hydrogen from high current densities in electroplating can cause hydrogen embrittlement unless proper baking procedures are used to allow the hydrogen to diffuse out. Electroplating can also cause high residual tensile stresses, which can contribute to crack initiation.

Welding can cause many different problems. These problems can be cracks that are initiated from improper welding procedures, high residual stresses, porosity from inadequately dried weld rods, or dirty workpieces. Microstructural notches or stress concentrations from the heat-affected zone and the transition to the base material can be the result of improper preheat and postheat. Improper weld penetration, weld geometry, and excessive weld current (undercutting) can also cause mechanical stress concentrations (Fig. 3).

The mast arm failure shown in Fig. 3 (Ref 2) was the result of weld bead undercutting and poor weldment design. Fatigue cracking initiated at the site of the weld toe undercut. This location was a highly stressed area and the location of a large mechanical stress-concentration factor because of the weld toe undercut. Typical

Fig. 2 Large gear that cracked during grinding operations. Localized thermal gradients during grinding resulted in high residual stresses and eventual cracking. Temper etching (dilute nitric acid in water) revealed the presence of abusive grinding.

© 2008 ASM International. All Rights Reserved.
Failure Analysis of Heat Treated Steel Component (#05113G) www.asminternational.org

Fig. 3 Failure of a mast arm due to fatigue that initiated at a weld toe undercut. Source: Ref 2

causes of undercutting include excessive weld current.

The assembly of a group of components can also cause eventual failure. Force-fitting a component creates high residual stresses or damage and causes premature failure to occur. Incorrect placement of a component or incorrect assembly order can also cause high residual stresses or failure to occur. Improper specifications or torque requirements can also cause premature failure. Misalignment of components within the assembly could also result in inadequate service life, because the stresses are not what the designer had anticipated.

Service conditions obviously can have a large role in the failure of a component. The service conditions could be normal operations but unanticipated by the designer. It could also be abnormal operations, such as speed, temperature (high or low), or a chemical environment, that were also unanticipated. The lack of proper scheduled maintenance can be a major contributor to premature failure. Maintenance procedures are often reduced as a cost-savings measure. Inadequate lubrication or improper lubrication can also play a role in failure (Fig. 4). In the case of Fig. 4 (Ref 3), the lubrication schedule was extended to reduce aircraft

Fig. 4 The probable cause of this accident was a loss of airplane pitch control resulting from the in-flight failure of the acme nut threads on the horizontal stabilizer trim system jackscrew assembly. The thread failure was caused by excessive wear resulting from insufficient lubrication of the jackscrew assembly. Source: Ref 3

© 2008 ASM International. All Rights Reserved.
Failure Analysis of Heat Treated Steel Component (#05113G) www.asminternational.org

downtime. This, and other contributing factors, resulted in the loss of 88 lives.

Stresses from startup can also contribute, along with rapid temperature gradients and rapid localized changes in the environment. Start-up procedures and maintenance are critical for intermittent operations. Shut-down procedures and resulting stresses are just as critical as proper startup. Inspection procedures to prevent failure are also important. Failure to properly inspect for problems or cracking can be catastrophic (Fig. 5), (Ref 4). In this case, maintenance and inspection personnel failed to detect a fatigue crack in the compressor stage of an aircraft engine. Upon application of power, the compressor stage ruptured, with shrapnel severing fuel lines and igniting the fuel, ultimately leading to the loss of the aircraft.

General Practice Conducting a Failure Analysis

The primary objective of any failure analysis is to determine the primary root cause of failure and to establish the appropriate corrective action. There are several stages of an analysis, which can proceed one after the other or occur at the same time. There is no set "fixed-in-stone" procedure, because it is highly dependent on the part and procedures/capabilities of the specific laboratory.

These stages of analysis are:

- Collection of background data
- Preliminary visual examination
- Nondestructive testing
- Selection and preservation of specimens
- Mechanical testing
- Macroexamination
- Microexamination
- Metallographic examination
- Determination of the fracture mechanism
- Chemical analysis (bulk and microanalysis)
- Exemplar testing
- Analysis and writing the report

Fig. 5 The probable cause of this accident was the failure of maintenance and inspection personnel to perform a proper inspection of a seventh-stage high compressor disk, thus allowing the detectable crack to grow to a length at which the disk ruptured under normal operating conditions, propelling engine fragments into the fuselage. The fragments severed the right engine main fuel line, which resulted in a fire that rapidly engulfed the cabin area. Source: Ref 4

These stages are described as follows, and additional information on failure analysis procedures is given in the chapter "General Aspects of Failure Analysis" in this book.

Collection of Background Information

During the collection of background data, the engineer is trying to gather an understanding of the purpose of the part. The engineer is attempting to discern the design criteria, service conditions, and failure conditions. In the background information, the operating details and manufacturing history should be examined and collected. This manufacturing history should include all the mechanical processing, thermal history or processing, and any chemical process performed on the part.

The service history should include all the maintenance records of the part. It should also include the expected environment and loading at the time of failure, as well as the normal environment and loading. Any quality records should be examined for discrepancies. Unfortunately, these records are not always available, and it is often up to the experience of the engineer to determine the quality of the part.

Preliminary Visual Examination

Documenting the failure or fracture is extremely important. There can never be too many drawings or photographs. The cost of photographs (especially digital) is cheap compared to analysis. A high-quality camera with macrocapability is very important and is one of the best tools that a failure analysis laboratory can have. The use of gray cards to ensure proper color rendition is also very important, because the color of scale or oxides can often give an indication of the temperatures that the part has experienced.

Sample selection is also very important. All associated debris should be collected and identified. Similar parts should also be collected for

© 2008 ASM International. All Rights Reserved.
Failure Analysis of Heat Treated Steel Component (#05113G) www.asminternational.org

comparison. In the case of a fastener failure, it is important that the nut and washer be collected, too. All mating pieces should be gathered for subsequent analysis.

Any abnormal conditions should be observed and compared with new and used components. Any discoloration or debris should be noted and collected. Any distortion of the part should be noted, along with dimensions of the part. Weather conditions at the time of failure should be collected, as well as all bearing and lubrication conditions and records.

During the initial wreckage analysis, the determination of all wreckage should be identified and located on a map or grid before any is touched or moved. Photograph each piece of wreckage and its surroundings. Inventory the parts present or missing. Determine the operating conditions at time of failure. This should include the position of control surfaces, power settings, position of throttles, and any lights or annunciations that occurred.

As best as possible during the initial examination of the wreckage, the sequence of failure should be determined. This can be accomplished by examining chevron markings and crack order. The parts should then be closely examined and reassembled. DO NOT allow the fracture surfaces to touch each other, because this can cause potential damage to the delicate surfaces. This analysis can also help determine the sequence of events leading up to failure. Preliminary examination of the part should note any paint, debris, or deposits present. Always remember to "do no harm."

The visual examination should be detailed. Fracture surface crack directions should be noted, identified, and documented. Any abuse or discoloration should be identified, and a general assessment of the workmanship should be determined. Document all findings with photography, with multiple photographs taken from different directions. The incorporation of rulers or scales is important to determine the size and direction of fracture.

Nondestructive Testing

Nondestructive testing is very useful for determining the extent of cracking. Magnetic particle inspection is useful for ferrous alloys, with dye-penetrant and ultrasonic inspection as additional methods available for initial inspection.

Magnetic particle inspection uses discontinuities in the magnetic field to identify cracks or discontinuities. Fluorescent dyes with small magnetic particles are used. These magnetic particles gather at the discontinuities in the magnetic field, indicating flaws or indications. It is a common, sensitive, and reliable method that is simple to learn and use. This method has no limitation in part size but is limited to magnetic materials. No elaborate precleaning of the surfaces is necessary. Detection is limited to the surface of the part or section examined. Care must be exercised to prevent local arcing.

The dye-penetrant method is useful for examining surface flaws or cracks. It is used primarily for nonferrous alloys but is used for examining ferrous weldments for cracks and porosity. In this method, a high-wetting liquid is spread on the surface of the part. Excess liquid is wiped off. A developer is applied to the part surface. Any cracks, flaws, or other indications will appear. Limitations of this method are the necessity of cleaning the surface prior to and after application of the indication fluid and developer solution. Surface features may also mask indications. It is simple to use, but an understanding of the limitations must be understood prior to application to a part.

Eddy-current methods depend on the principle that all metals conduct electricity. An alternating current is applied, and eddy currents occur by electromagnetic induction. Cracks or other flaws cause distortions in the electromagnetic fields, with a result of changing the field impedance. The advantage of this method is that subsurface discontinuities can be detected. No special skill is required to use this method, and the method can be automated. Probe contact with the part is not needed. Limitations of this method are that the depth penetration is limited, and the part must be capable of conducting electricity. Reference standards are needed for specific flaw sizes and materials. Many things can influence readings, including segregation, carburized layers, and changes in profile.

Ultrasonic testing uses high-frequency sound waves transmitted through a conducting medium. Any discontinuous boundary can cause a deflection. This method is very sensitive and has high penetration. It is possible to get accurate measurements of flaw position and size, but reference standards must be used. Shape and size can cause errors in interpretation. Experienced operators are required to properly interpret the

© 2008 ASM International. All Rights Reserved.
Failure Analysis of Heat Treated Steel Component (#05113G) www.asminternational.org

results of testing. Effects of grain size, porosity, and inclusions can also hinder interpretation.

Radiography, using x-rays, neutrons, or gamma rays, is also often used to examine structures. Film or sensors (charge-coupled devices) pick up the emitting radiation, with the intensity proportional to the density of the sample. Light areas indicate a dense region, and dark areas indicate a greater exposure or less dense region. Advantages of radiography are the detection of subsurface and internal features at various depths and the documentation of these features by film or other imaging techniques. The primary disadvantage is that reference standards must be used, and the area for testing must be enclosed to prevent radiation from leaking out.

Mechanical Testing

Mechanical testing is useful to determine the properties of the part and to verify that it meets expected properties and specifications. There are many types of mechanical testing available, including hardness, tensile testing, and impact fracture testing.

Hardness testing is probably the most versatile and widely used. It is often used to evaluate heat treatment and can be used as an approximation for tensile strength. It can be used to detect the presence of work hardening or softening and hardening or softening from localized thermal events such as grinding. For the most part, it is a nondestructive test. For microhardness testing, it is necessary to use a metallographic specimen.

Tensile testing is used more to establish conformance to specification. It is not necessary to show inadequate ductility because of service loads. Because of the size of the tensile specimen, it may not be possible to excise an appropriately sized sample from the part. Anisotropy of properties can be expected to lower measured tensile and yield strength properties.

Impact and fracture toughness testing is typically used to determine conformance to specifications. Charpy impact testing has a high variability in results and may be temperature related. Results must be taken with temperature in mind and may not correlate with real results because of size limitations. Fracture toughness testing and the results from K_{Ic} testing can be used in design, and the results are useful for calculating critical flaw sizes. It can also be used to examine estimated crack growth rates; however, samples are difficult to prepare and test. These methods also do not incorporate the effects of residual stresses.

Selection and Preservation of Specimens

The selection and preservation of fracture surfaces is vital to prevent the destruction of evidence. Unprotected, the fracture surfaces or parts can become mechanically or chemically damaged. This damage can obliterate evidence and make the determination of fracture difficult or impossible. Both sides of the fracture must be protected. This is in the event that if one surface is damaged, the other side can be examined. Protection of the specimens during shipment is also very important, because evidence could be destroyed. Avoid touching surfaces with the hands, because the chemicals and acids present can cause artifacts or destroy data. NEVER fit surfaces together, because the delicate fracture features can be destroyed. Since both surfaces would be damaged, it could destroy the chances for determining the fracture mechanism.

Cleaning of specimens is to be done only when absolutely necessary. For the most part, it is required to prepare the sample for the scanning electron microscope (SEM). Dry air blasts or soft artist brushes are typically all that is needed. Rinsing in organic solvents then evaporating the solvent with dry air is useful for preparing specimens for the SEM.

Chemical cleaning is generally not recommended under any circumstance. Foreign substances such as scale or debris should be preserved. Do not use rust inhibitors, because of the inevitable damage to the part and fracture surfaces. These rust inhibitors are also extremely difficult to remove. Avoid washing the sample or parts with water unless seawater or other chemical is present. In this case, gently wash with distilled water and follow that with high-quality alcohol or acetone. Allow to dry and place in a dessicator.

Plastic replicas are useful in preserving fracture surfaces and removing debris for further analysis. Softening replica tape (available at transmission electron microscope supply houses) with small amounts of acetone forms plastic replicas. The softened tape is pressed gently onto the fracture surface. Additional layers of tape, softened with acetone, are applied to the fracture surface. After multiple layers have been applied, the entire replica is allowed to dry and then is placed in a dessicator. When the part is ready to be examined, the replica is

© 2008 ASM International. All Rights Reserved.
Failure Analysis of Heat Treated Steel Component (#05113G) www.asminternational.org

carefully removed using tweezers. Any debris on the surface is also preserved for further analysis in the replica. Multiple plastic replicas can be used to clean a surface of a part. This can be repeated as necessary.

Sectioning of Specimens

Sectioning is very important, because it captures the portion of the fracture surface for examination or the appropriate metallographic specimen. The biggest limitation is size. It is important that the portion to be removed is documented by photographs and sketches, showing the location of the specimen to be removed. Preserve any fracture surface by plastic replicas or other method to prevent damage or attack. Regions adjacent to cracks are also to be preserved and protected. Cutting the specimens should be done very carefully so as not to cause any heat damage. Coolants are not recommended, unless the material cannot be cut without heat generation. The use of plastic replicas is useful for protecting surfaces and preserving any debris present.

Opening secondary cracks is useful when the primary fracture surface is damaged. These secondary cracks may provide better information, because they are tightly closed, and the fracture surfaces are not exposed to surface contaminants and corrosion. Care must be taken not to damage the primary fracture surface. Bending to open the crack is preferable, to expose the crack face. Often, the use of a sawcut to the back of the part will reduce the amount of force necessary to open the secondary crack. Another method is to use a tensile machine to open the crack face. The crack opening should be measured prior to opening, and the crack opening displacement can also be measured as the crack is slowly opened and exposed. One technique is to immerse the specimen in liquid nitrogen and impact the part so that the fracture surfaces are rapidly opened. One problem with this method is that it is very easy to damage the fracture surface from a misapplied hammer hit.

Macroscopic Examination

The macroscopic examination is conducted by a detailed examination at 1 to 100× by eye or binocular microscope. High-quality optics with excellent depth of field are required to properly examine the fracture surfaces. This detailed macroscopic examination can reveal a wealth of information on the location of fracture origins, direction of cracking, configuration of the stress state, and the last region to fail (shear lip). The presence of chevron marks can indicate the direction of rapid crack growth, and the different textures of the fracture can differentiate between fast final fracture and the initiating mechanism of fracture. Different textures from the region of fast fracture can indicate a different mechanism, such as fatigue, stress-corrosion cracking, or hydrogen embrittlement.

Microscopic Examination

The microscopic examination is usually conducted with an SEM (Fig. 6). This instrument is probably the most useful of all instruments for determining the mechanism of failure. It is capable of a large depth of field, with magnifications of 10 to 300,000×. It allows for direct examination of specimens, and when coupled with an energy-dispersive spectrometer, very small regions can be examined and analyzed for chemistry. It is very easy to use and requires very little training to take quality images.

Interpretation of the images requires experience and understanding of the four basic modes of failure: dimpled rupture, cleavage, brittle intergranular, and fatigue. From these four basic modes, the detailed mode can be examined, and the failure mechanism is fit to the evidence. A greater discussion of the mechanisms of failure is found later in this chapter and elsewhere in this book.

Metallography

Metallography is a vital part of a failure analysis investigation. It can examine crack

Fig. 6 Typical scanning electron microscope used for microscopic analysis of a fracture surface

© 2008 ASM International. All Rights Reserved.
Failure Analysis of Heat Treated Steel Component (#05113G) www.asminternational.org

morphology and its relationship with the microstructure present. It can help determine the thermal history of a component or region of a part and can show if work hardening was present. There can never be too many photographs and metallographic sections. Metallographic sections should be taken away from the crack and near the determined origins of cracking. Because this method is destructive, it is undertaken last. Typically, the crack face and edges are protected from rounding by applying support. This support can be electroless nickel plate or the use of alumina beads or steel shot in the metallographic specimen, adjacent to the surface.

Metallographic specimens are prepared using an epoxy or phenolic resin. The sample is placed into a small press, and phenolic resin is poured over the section. The press compacts the resin and forms a small, round sample that is then polished, etched, and examined under a metallographic microscope. When the specimen has cooled, it is taken out of the press and ground through a sequence of sandpapers. Typically, the sequence is 240, 320, 400, and 600 grit. The specimen is ground very flat before polishing. During polishing, the metallographic specimen is polished using a flat platen and 3 μm alumina slurries. Final polish is accomplished using 0.15 μm alumina slurry. Other polishing agents can be used, with diamond being a very common polishing agent. A finished metallographic sample used for the determination of the fracture mechanism in a steel weldment is shown in Fig. 7.

Examination of the metallographic specimen reveals surface imperfections, inclusions, and microstructural details. It can reveal the presence of decarburization and improper heat treatment. It often provides the needed documentation and support for the fracture analysis and determination of the root cause of failure.

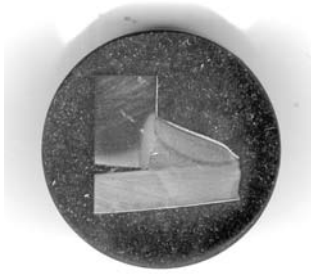

Fig. 7 Typical metallographic specimen. This specimen was used to examine microstructures in a failed weldment.

Determination of the Fracture Mechanism

Examination of the fracture surface and metallography are used to determine the cause of failure. First, it is necessary to determine the fracture mode. Unfortunately, there is no clear or logical classification of fracture. Generally, classification is based on the crack growth mechanism (see also the chapter "General Aspects of Failure Analysis" in this book).

Ductile Fracture

On a macroscopic scale, a ductile fracture is accompanied by a relatively large amount of plastic deformation before the part fails. After failure, the cross section is reduced or distorted. Shear lips are observed at the latter part of the fracture and indicate the final failure of the part. The fracture surface is dull, with a fibrous appearance. Microscopically, ductile fracture is characterized by several distinct stages (Ref 5–8); an example is shown in Fig. 8. In this case, an ISO 12.9 low-alloy bolt failed by ductile torsional overload. The fracture was smooth, with fracture initiating from the threads. The fracture mode was microvoid coalescence (Ref 9), which occurs by the following process:

- A free surface is created from a small particle. This particle can be a second-phase particle, dispersoid, or inclusion. The separation of the metal matrix from the small particle at the matrix/particle interface can form this free surface, or the fracturing of the small particle can form the free surface.
- The free surface around the small particle creates a void. This void grows by plastic strain and hydrostatic stress.
- Finally, the voids grow to a size that they join or coalescence with adjacent voids.

This process of void formation, growth, and coalescence is shown schematically in Fig. 9. If the particles are well matched to the matrix and form a strong interface between the matrix and the particle, then the initial formation of voids is the critical step. Fracture occurs shortly after

© 2008 ASM International. All Rights Reserved.
Failure Analysis of Heat Treated Steel Component (#05113G) www.asminternational.org

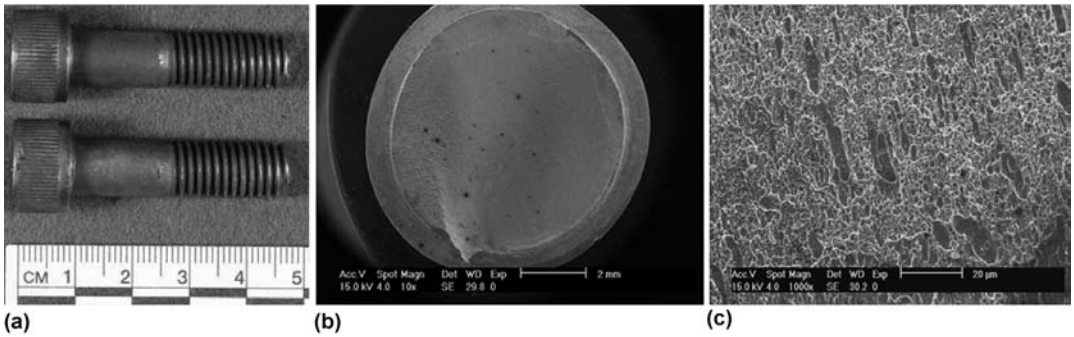

Fig. 8 Fracture of an ISO 12.9 bolt by ductile torsional overload. (a) Overall view of fracture. (b) Smooth and fibrous fracture as seen through the SEM. (c) Microvoid coalescence (dimples)

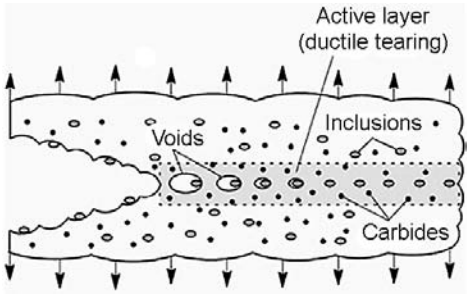

Fig. 9 Schematic showing the formation of microvoid coalescence

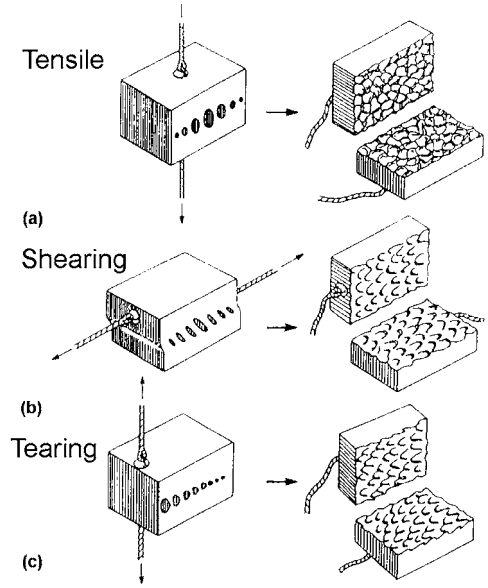

Fig. 10 Schematic representation of the creation of dimples in a loaded member by (a) simple tension, (b) shear loading, and (c) tearing

void formation (Ref 10). If the interface between the particles and the matrix is weak, then voids form and grow readily. Substantial plastic deformation occurs. Fracture occurs when the voids reach a critical size. These voids substantially reduce the cross section, with the resulting local plastic instability (Ref 11). These voids coalesce to form a central crack perpendicular to the applied tensile stress. Depending on the applied stresses, the shape and configuration of the dimple shape can be changed (Fig. 10). This fact is important in determining the type of loading during a postfracture investigation. Dimples are small and can only be detected by using electron microscopy (Fig. 11).

The presence of inclusions in steel plays a major role in the ductility of steel. As indicated previously, the inclusions fracture and separate from the matrix during decohesion. Therefore, the deformability of these inclusions is important to determine the ductility of steel.

Nearly all steels have nonmetallic inclusions. The size and frequency of these inclusions is determined by the methods described in ASTM E45 (Ref 12). The cleanliness of the steel is

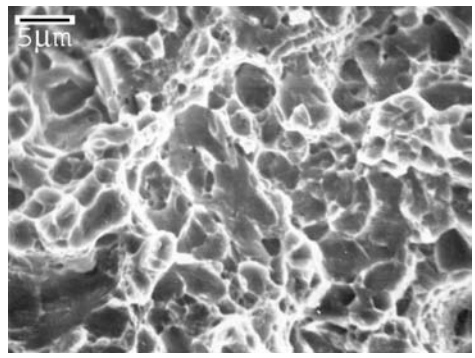

Fig. 11 Microvoid coalescence as seen through the SEM

© 2008 ASM International. All Rights Reserved.
Failure Analysis of Heat Treated Steel Component (#05113G) www.asminternational.org

important to the ductility of the steel. All other things being equal, the steel with the lower inclusion size, shape, and frequency will have a greater ductility than another steel with a greater inclusion count. Modern steelmaking practices generally produce low inclusion content. Often, steels for aerospace applications require a frequency/severity determination of inclusions in accordance with AMS 2300, AMS 2301, AMS 2303, or AMS 2304 (Ref 13–16). A specific-sized test specimen must be heat treated and examined using magnetic particle inspection. The procedures are outlined in the aforementioned specifications.

The inclusions found in steels have been divided into five categories related to their deformation behavior (Ref 17):

- The inclusions Al_2O_3 and calcium aluminates are produced during deoxidation of steel during the production of molten steel. They are brittle at practically all temperatures.
- Spinel-type oxides are not deformable up to 1200 °C but may be deformed above this temperature.
- Silicates of calcium, manganese, iron, and aluminum in various proportions are brittle inclusions at room temperature but become more deformable at higher temperatures. The formability increases as the melting temperature of the silicate decreases. Therefore, aluminum silicate has much less formability than the lower-melting manganese silicates.
- FeO and (FeMn)O are deformable at room temperature but gradually become more brittle at temperatures above 400 °C.
- Manganese sulfide (MnS) is the most common inclusion found in steel, and it is increasingly deformable as the temperature falls. The morphology of the MnS inclusions changes, depending on how they were formed.

Ductile failure can occur with any of the types of inclusions. This is true whether it is the brittle alumina-type inclusions or the more ductile sulfide-type inclusions. Inclusions generally initiate ductile cracking above a critical size. Coarser inclusion sizes tend to have a larger local stress-concentration factor, which can cause local decohesion and microcrack formation. Work by Maropoulos and Ridley (Ref 18) has shown the effect of volume fraction of iron-alumina on the ductility of steel. Increasing amounts of inclusions reduce the ductility of the steel. A reduction in the yield stress, due to the stress concentrations around the inclusions, is evident at low volume concentrations of inclusions.

The presence of inclusions in the size range of 1 to 30 μm reduces the energy absorbed during ductile fracture. Fine dispersions of ductile inclusions will delay the onset of cleavage-type fracture by localized relaxation of stresses. At the same time, the yield stress also increases.

During deformation, forming, or forging, the ductile inclusion MnS has a marked effect on the ductility of the final product. Types 1 and 2 MnS inclusions will elongate on deformation, while type 3 MnS inclusions will rotate into the rolling plane. This will reduce toughness and ductility in the transverse direction. Type 2 inclusions are the most harmful to ductility and toughness, so some effort is being made to eliminate these inclusions by ladle additions of other strong sulfide formers, such as titanium, zirconium, and calcium.

Ductility is also influenced by the fact that MnS contracts more than the iron matrix upon cooling. The bond between the MnS inclusion and the matrix is not strong enough to prevent microvoid formation. Because MnS inclusions tend to form as strings or stringers along the rolling direction, the toughness and ductility are strongly influenced in the rolling direction. Transverse to the rolling direction, ductility and toughness are much worse.

In a similar fashion to that of inclusions, the distribution of carbides can also influence the toughness and ductility of the steel. The strain needed for void formation decreases with increasing carbide volume fraction. Spheroidal carbides will not crack at small strains and exhibit decohesion. Spheroidized steel is much more ductile than similar steel of the same hardness containing only ferrite and pearlite. Pearlite has a lower critical strain for void formation. In addition, when a crack or void forms in a pearlitic matrix, it will tend to run along the length of a pearlite lamella. Examining this type of fracture under the SEM reveals that the base of the dimples contain fractured pearlite lamella.

Brittle Fracture

Very little plastic deformation and a shiny fracture surface characterize brittle fractures. Often, chevron patterns point back to the origin

© 2008 ASM International. All Rights Reserved.
Failure Analysis of Heat Treated Steel Component (#05113G) www.asminternational.org

of failure (Fig. 12) (Ref 19). It can occur at low stress and propagate with rapidity, often at speeds approaching the speed of sound in the failed material.

Since the early 1940s, there has been tremendous growth in the number of large welded structures. Many of these structures have failed catastrophically in service, most notably the "Liberty ships" (Ref 20) used to transport war material during World War II. Analysis of the fracture surfaces of the failures (Ref 21) indicated that they initiated at a notch and propagated with no plastic deformation. These notches were of three types:

- *Design features:* Structural members were rigidly joined at angles less than 90° and then welded.
- *Fabrication details:* Procedures used during the manufacture of the part caused the formation of notches. Welding arc strikes, gouges, and fitting procedures created physical notches. Welding procedures and heat treatment caused metallurgical or microstructural notches to occur from abrupt changes in microstructure or the production of microstructures that were brittle. Features such as porosity from welding or casting also caused brittle fracture initiation.
- *Material flaws:* These flaws resulted from melt practice at the mill and appeared as large inclusions, internal oxidation, porosity, or segregation.

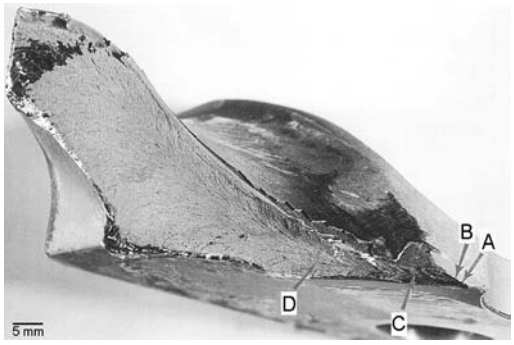

Fig. 12 Chevron markings point back to the origin of failure in brittle steels. Source: Ref 19

In brittle fractures, limited energy is absorbed by the fracture. Energy is absorbed through regions of small plastic deformation. Individual grains separate by cleavage along specific crystallographic planes. This is shown in Fig. 13.

Visually, little or no plastic deformation or distortion of the shape of the part characterizes brittle fractures. The fracture is usually flat and perpendicular to the stress axis. The fracture surface is shiny, with a grainy appearance. Failure occurs rapidly, often with a loud report. Because the brittle cleavage is crystallographic in nature, the fracture appearance is faceted. Often, other features are present, such as river patterns (Ref 23). These are shown schematically in Fig. 14.

There are three basic factors that contribute to a cleavage type of fracture in steels. They are:

- Triaxial stress state that forms at a notch, similar to that described previously
- Low temperature
- High strain rate or rapid loading rate

These three factors do not have to be present for cleavage-type fracture to occur. Most brittle, cleavage-type fractures occur when there is a triaxial stress state and low temperature. This is

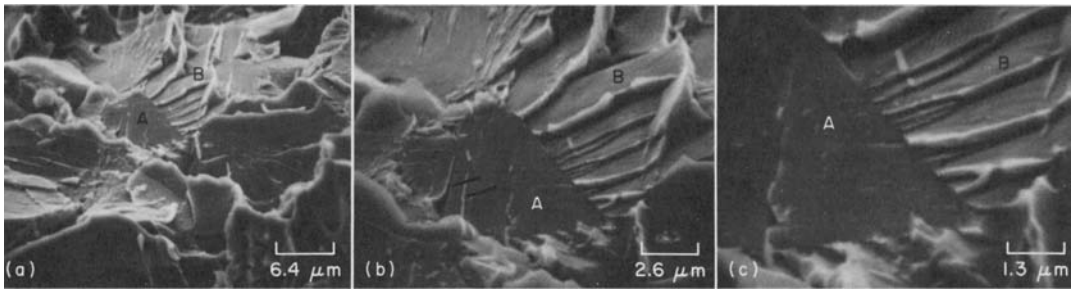

Fig. 13 Cleavage fracture in a low-carbon steel, seen through an SEM. Cleavage fracture in a notched impact specimen of hot-rolled 1040 steel broken at −196 °C (−320 °F), shown at three magnifications. The specimen was tilted at an angle of 40° to the electron beam. The cleavage planes followed by the crack show various alignments, as influenced by the orientations of the individual grains. Grain A, at center in fractograph (a), shows two sets of tongues (see arrowheads in fractograph b) as a result of local cleavage along the {112} planes of microtwins created by plastic deformation at the tip of the main crack on {100} planes. Grain B and many other facets show the cleavage steps of river patterns. The junctions of the steps point in the direction of crack propagation from grain A through grain B, at approximately 22° to the horizontal plane. The details of these forks are clear in fractograph (c). Source: Ref 22

© 2008 ASM International. All Rights Reserved.
Failure Analysis of Heat Treated Steel Component (#05113G) www.asminternational.org

actuated by a high rate of loading. Many types of tests have been developed to determine the susceptibility of steels to brittle behavior. These tests include the Charpy impact test (ASTM E23) (Ref 24) and the fracture toughness test (ASTM E399) (Ref 25). Others include the nil-ductility test (ASTM E208) (Ref 26) and dynamic tear test (ASTM E604) (Ref 27).

The notch toughness of low- and medium-strength steels is highly dependent on temperature. There is a transition from ductile fracture to brittle fracture as the temperature decreases. One criterion for the transition temperature is the nil-ductility temperature (NDT). The NDT is the temperature where fracture becomes 100% cleavage, and there is essentially no plastic deformation.

Changes in the NDT can be produced by changes in microstructure and chemistry. The largest change can be effected by changes in the amount of carbon and manganese. The NDT is lowered by approximately 6 °C (10 °F) for every 0.1% increase in the manganese concentration. Increasing the carbon content also lowers the NDT. The manganese-carbon ratio should be approximately 3 to 1 for good notch toughness.

Decreasing the concentration of phosphorus also decreases the NDT. Nitrogen causes the NDT to increase (more brittle). However, because of the interaction with other alloying elements in steel, it is difficult to quantify the increase of NDT with increasing nitrogen concentration.

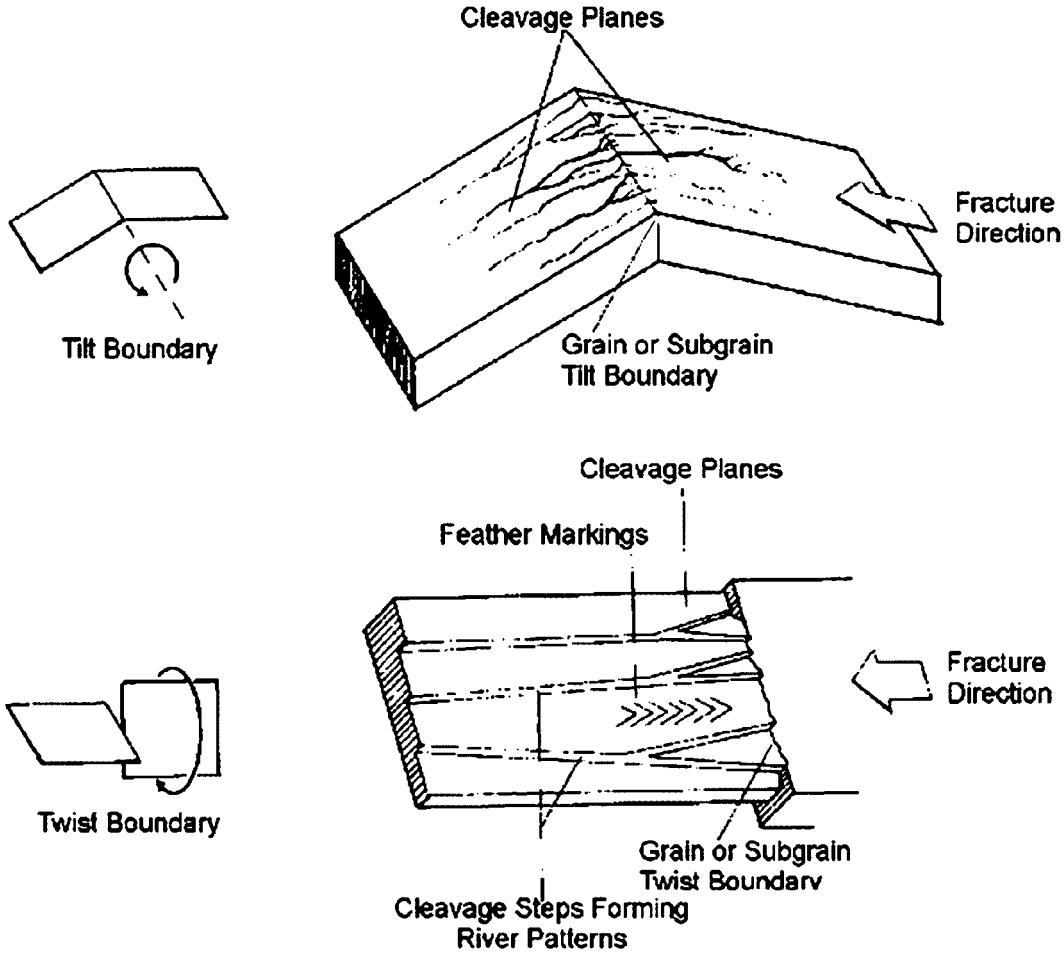

Fig. 14 Schematic of river patterns formed in brittle materials. (a) Tilt boundary. (b) Twist boundary. Source: Ref 23

© 2008 ASM International. All Rights Reserved.

Nickel is beneficial for increasing ductility. Up to 2% Ni is effective in lowering the NDT. Increasing concentrations of silicon have the effect of increasing the NDT. Chromium has nearly no effect, while molybdenum is extremely effective in increasing the ductility of steels and drastically decreasing the NDT. Oxygen strongly decreases the ductility. It can also cause an increased propensity for intergranular fracture by creating brittle oxides at the grain boundaries. Decreasing the grain size has a strong effect on increasing the ductility and notch toughness.

Section thickness can also influence ductile and brittle behavior (Ref 28). The results showed that there was considerable variation of toughness with the thickness of the specimen (Ref 29, 30). Further, at large thickness, the toughness appeared to reach a constant value (Fig. 15) (Ref 31). Within this curve, there are three apparent regions. First, there is the region where maximum toughness is obtained (thin sections). Second, there is the region of intermediate toughness, and lastly, a region with relatively constant toughness (thick sections).

In the first region, the fracture appears to consist entirely of a shear lip, or, in other words, the fracture surface is inclined at an angle of approximately 45° to the tensile axis. In this situation, the stress in the direction of the thickness of the specimen tends toward zero, and a state of plane stress is achieved. As the specimen is pulled, it experiences buckling. Because of this buckling, yielding occurs on the through-thickness planes at an angle of 45° to the tensile axis. Crack extension occurs by sliding. This sliding motion is achieved by the movement of a number of screw dislocations (Ref 32, 33) on the 45° plane, as shown in Fig. 16.

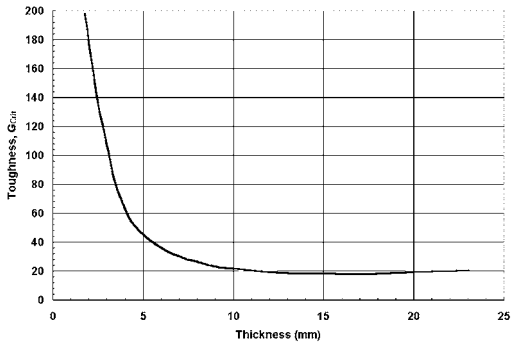

Fig. 15 Variation of toughness with thickness

In the intermediate range, the fracture behavior is complicated. The fracture does not consist of entirely slant-type fracture, nor does it contain entirely a flat plane-strain-type fracture. Instead, the regions of flat and slant fracture are approximately equal. At the thin end of the thickness range, the slant ligaments on either side of the testpiece carry most of the load. At the thick end of the range, the side ligaments carry a much smaller percentage of the load. The amount of flat fracture increases. This is shown schematically in Fig. 17. It has been found (Ref 28) that the amount of flat fracture depends only on the thickness of the test specimen and was independent of crack length.

In the third region, the fracture consists of predominantly flat fracture. Some evidence of very small shear lips may be present at the later part of fracture. Fracture is catastrophic and rapid. No plastic deformation is evident. In this third region, any increase in the thickness of the testpiece causes no further decrease in the toughness.

These fracture patterns are useful in determining the state of stress within a failed component and can help to understand the mechanism of failure.

One famous failure involving brittle fracture was the "Great Boston Molasses Disaster"

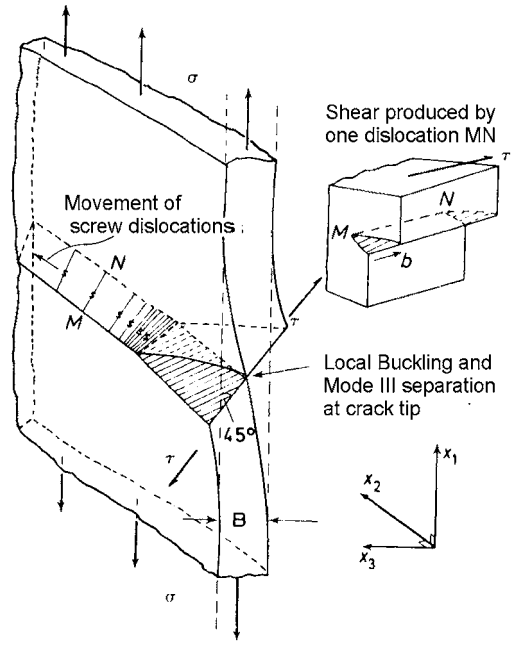

Fig. 16 Mode of separation in a thin sheet

© 2008 ASM International. All Rights Reserved.
Failure Analysis of Heat Treated Steel Component (#05113G) www.asminternational.org

(Ref 34). In this failure, the United States Alcohol Company fabricated a large cast iron molasses tank in Boston in December 1915. This tank was 27 m (90 ft) wide and 17.7 m (58 ft) tall, with a head of 15 m (49.5 ft) of molasses. It was fabricated of cast iron plates riveted together. It held 8.7×10^6 L (2.3 million gal) of molasses, ostensibly used for the fermentation of ethanol used for liquor. The man who oversaw construction could not read blueprints, nor did he have any technical training. No engineers or architects were consulted to ensure that the tank was constructed safely. On January 15, 1919, the tank exploded with great force, and the streets of Boston were flooded with waves of molasses from 2 to over 4 m (8 to 15 ft) tall (Fig. 18). This great wall of molasses was reported to have moved at speeds up to 35 miles (56 km) per hour and devastated a large section of Boston along Commercial Street between Copps Hill and the playground of North End Park. Half-inch steel plates were torn apart, and these plates were thrown with enough force to cut girders of the elevated railway. This explosion, and the subsequent wave of molasses, resulted in 21 people killed, 150 people injured, many buildings destroyed, and an entire area devastated. The elevated train trestles were knocked over. Early accounts of the disaster included reports that the tank was destroyed by anarchists. In a trial, it was found that the company was liable for $628,000 in damages (in 2007 dollars, approximately $7,000,000). Investigation many years later indicated that the probable cause was brittle fracture of the tank at the rivets, with the temperature below the ductile-to-brittle transition temperature. One interesting result of this disaster was that Massachusetts and many other states created laws to certify engineers and to regulate construction. It also required stamped drawings certifying that an engineer had reviewed the plans. It was this failure that was the origin of the professional engineer's license and stamp, as it is known today (2007). As a side note, the 18th Amendment was ratified and Prohibition signed into law on January 16, 1919.

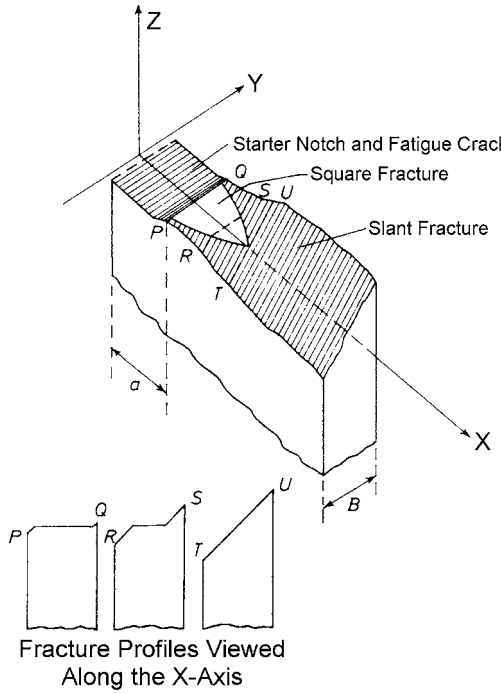

Fig. 17 Schematic of fracture in the intermediate range

In another example of brittle fracture, an AISI 4330V hook-point, used for the arrestment of

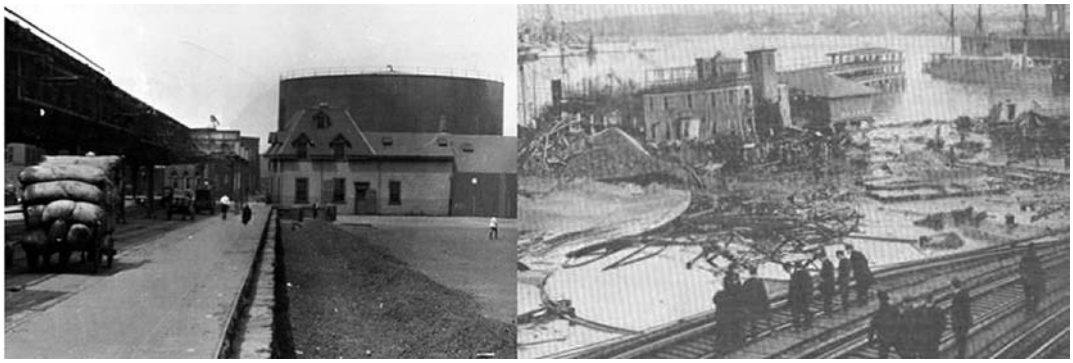

Fig. 18 The Great Boston Molasses Disaster. Twenty-one people were killed and over 150 buildings destroyed as the result of 2.3 million gal of molasses flooding North Boston.

© 2008 ASM International. All Rights Reserved.

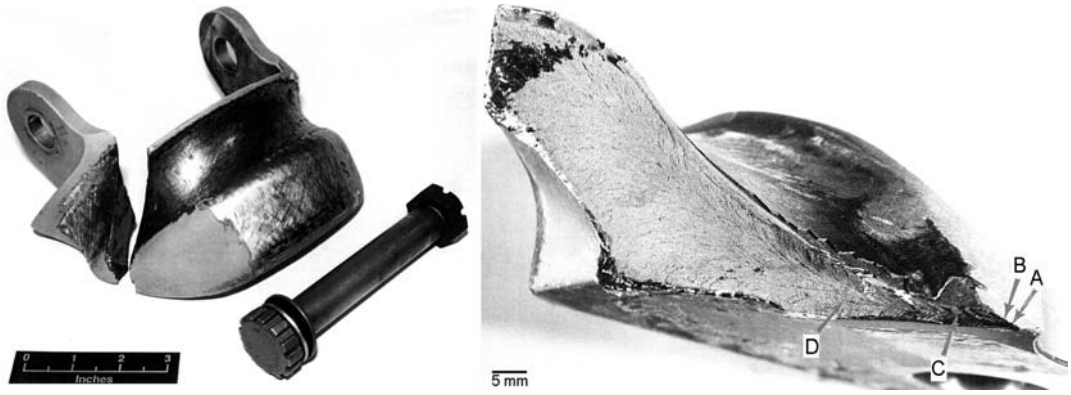

Fig. 19 Arresting gear hook-point, manufactured from AISI 4330V, that failed during landing. Failure occurred at the inner fillet radius of the right-hand lug

naval aircraft on landing, failed during field trials during the 13th arrestment. The landing configuration was severe, with high aircraft sink rates, high aircraft gross weight, and landing at a large angle to the cable. The hook-point failed at the inner fillet radius of the right-hand lug (Fig. 19). The hook-point successfully engaged the arrestment cable, with no other aircraft damage. The part was forged, machined, heat treated, and hard surfaced in the cable groove, using a high-velocity oxyfuel coating for wear resistance. Examination showed that the microstructure of the hook-point was quenched and tempered martensite. Hardness measurements showed that the hook-point had a substantially higher hardness (HRC 54) than the specified hardness of HRC 46 to 48. The chemistry of the hook-point indicated that it was at the high side of the specification, increasing the hardenability of the steel and increasing the resistance to tempering. Hydrogen measurements indicated that the hydrogen content was 0.2 ppm. The high strain rate during landing and the low concentration of hydrogen precluded failure by hydrogen embrittlement. An SEM examination of the fracture surface showed that the fracture contained microvoid coalescence and quasi-cleavage, suggestive of brittle failure (Fig. 20). Charpy impact testing showed that the impact toughness of the as-received part was significantly lower than a part of the same chemistry properly tempered to HRC 46. Finite element analysis showed a high localized stress concentration at the lug inside fillet radius. It also showed that the stresses were highly triaxial. Based on the analysis, it was determined that the hook-point lug failed by quasi-cleavage,

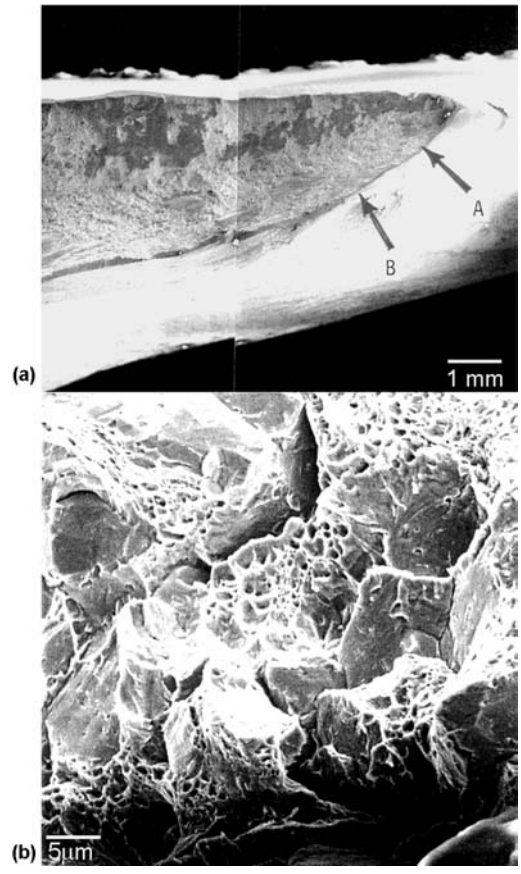

Fig. 20 SEM fractographs showing (a) location of origin at the inner fillet radius and (b) quasi-cleavage evident on the fracture surface

and that the failure was aggravated by high local stress concentration at the fillet radius, improper heat treatment (making the material more

© 2008 ASM International. All Rights Reserved.
Failure Analysis of Heat Treated Steel Component (#05113G) www.asminternational.org

brittle), and extremely high dynamic loading. It was recommended that the radius be made larger to reduce the stress concentration and also to retemper the hook-points to meet specification.

Intergranular Brittle Fracture

Another form of brittle fracture is called intergranular cracking. In this fracture mechanism, failure occurs by decohesion along grain boundaries and not on specific crystallographic planes, such as in cleavage fracture. Intergranular cracking can have several different causes. Typical causes of intergranular cracking in steel alloys include:

- *Quench-age embrittlement:* Cooling of carbon steels and low-alloy steels from subcritical temperatures can precipitate carbides within the microstructure. The strength is raised, but toughness is lost.
- *Quench cracking:* During quenching, the transformational and residual stresses developed during quenching of steels can cause cracking during heat treatment.
- *Tempered martensite embrittlement:* Within the range where blue-purple oxides can form on steels (230 to 370 °C, or 450 to 700 °F), precipitates can form that increase the tensile strength and hardness while reducing the ductility and toughness.
- *Temper embrittlement:* Quenched steels containing appreciable amounts of manganese, silicon, nickel, or chromium are susceptible to temper embrittlement if they contain even trace amounts of antimony, tin, or arsenic. Embrittlement of susceptible steels can occur after heating in the range of 370 to 575 °C (700 to 1070 °F) but occurs most rapidly at approximately 450 to 475 °C (840 to 885 °F).
- *Graphitization:* This happens when the pearlite in steels begins to decompose into ferrite and graphite following very long, high-temperature service, for example, in steam power stations. For these applications, a few steels turn out to be satisfactory, while many others are subject to graphitization.
- *Internal oxidation:* This is one of the common failures in high-temperature, oxidizing conditions.
- *Liquid metal embrittlement or solid metal embrittlement:* Intermetallic compounds form at grain boundaries when low-melting-temperature metals (cadmium, zinc, etc.) penetrate by diffusion. An example would be galvanized steel where the zinc has diffused into the steel in the vicinity of 420 °C (787 °F).
- *Hydrogen embrittlement:* The presence of hydrogen and static loads or a low strain rate can result in hydrogen embrittlement.
- *Stress-corrosion cracking*
- *Grain-boundary decohesion at elevated temperatures (creep rupture)*

The fracture surface appearance of intergranular cracking is generally shiny and faceted. It has a "rock-candy" appearance. Often, when the mechanism is from corrosion, the corrosion product is present. This can dull the appearance of the facets. The appearance of intergranular fracture is most clearly seen in the electron microscope, and an example is shown in Fig. 21.

Quench cracking is the limiting case of excessive residual stresses exceeding the tensile strength of the material. Two processes contribute to quench cracking, as well as distortion and residual stresses. The first process is the stress from the volume expansion of martensite during transformation from austenite to martensite. The second source is from thermal stress due to differential contraction due to different cooling rates in the steel. The transformational stress from the formation of martensite is primarily responsible for cracking during quenching, and thermal stresses from differential cooling are usually from subcritical heat treatments such as annealing.

During quenching, the volume expands from the close-packed face-centered cubic structure of austenite to the body-centered tetragonal structure of martensite. This volume expansion

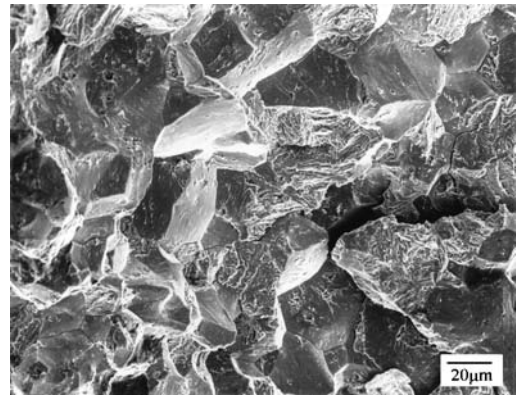

Fig. 21 Intergranular fracture from hydrogen embrittlement, as seen through the SEM

© 2008 ASM International. All Rights Reserved.

is approximately 4% and is related to the carbon content of the steel. During quenching, the outer surface of the part cools first and transforms to martensite. There is an attendant volume expansion at the surface, and the untransformed and still hot interior surface usually has sufficient plasticity to accommodate the changes in the part volume. The outside surface is in compression. Upon cooling, the interior of the part also transforms to martensite but is constrained by the hard outside surface layer of previously transformed martensite. On the transformation of the inner core, a volume expansion occurs in the interior of the part, and the outer surface is placed in tension. If quenching is severe, the resulting tensile residual stresses can exceed the ultimate tensile stress of the surface untempered martensite. Cracking is intergranular and often exhibits an oxide scale on the fracture surface. If cracking occurred during quenching, remnants of quench oil can be found on the surface of the crack, and often, elevated-temperature scale is apparent. Cracking can be delayed due to the transformation of retained austenite. This is one reason why it is recommended to temper parts immediately after quenching. Should delayed quench cracking occur, then the temper scale is thinner and often shows the characteristic temper colors, indicative of the temper temperature. High-carbon steels and steels with high hardenability are the most prone to quench cracking.

Surface features such as sharp radii, large changes in section, or the presence of laps, burrs, rough-machined surfaces, and other surface discontinuities increase the constraint during quenching and increase the propensity toward quench cracking.

Quench cracking can be mitigated by improved surface condition and the removal of scale, burrs, and sharp edges. Geometry changes, by increasing transitions from thin to thick sections, and generous radii can also help reduce quench cracking. The use of higher-hardenability alloys will also reduce the propensity for cracking, because it will allow a reduced quench rate to achieve the same properties. Reducing the austenitizing temperature or reducing the temperature differential between the austenitizing temperature and the quenchant temperature will reduce the propensity for cracking. Often, the geometry is set, as is the alloy of the part. In this case, the heat treater can reduce the quench rate or use martempering to reduce quench cracking.

Martempering is the process of using high-temperature quench oils and quench oil temperatures of 90 to approximately 200 °C (200 to 400 °F). The part is quenched into the high-temperature oil, and the parts are allowed to equilibrate or at least minimize the temperature gradient across the interior of the part. The part is then removed from the oil and allowed to cool in any convenient manner. This method has proven to be very effective in reducing quench cracking as well as distortion from quenching.

A long pinion gear failed in service near the midlength of the shaft (Fig. 22). One gear tooth fractured during service, resulting in the gear being removed from service and sent to the laboratory for failure analysis. Magnetic particle inspection, using a fluorescent dye, revealed the presence of multiple linear indications on cracking of the gear tooth faces (Fig. 23). Examination of the fracture surface showed a discolored region at the origin of cracking (Fig. 24). This discolored region was attributed

Fig. 22 As-received pinion gear that failed in service

Fig. 23 Magnetic particle inspection of the failed pinion gear showed arc-shaped cracks on the gear tooth faces.

© 2008 ASM International. All Rights Reserved.
Failure Analysis of Heat Treated Steel Component (#05113G) www.asminternational.org

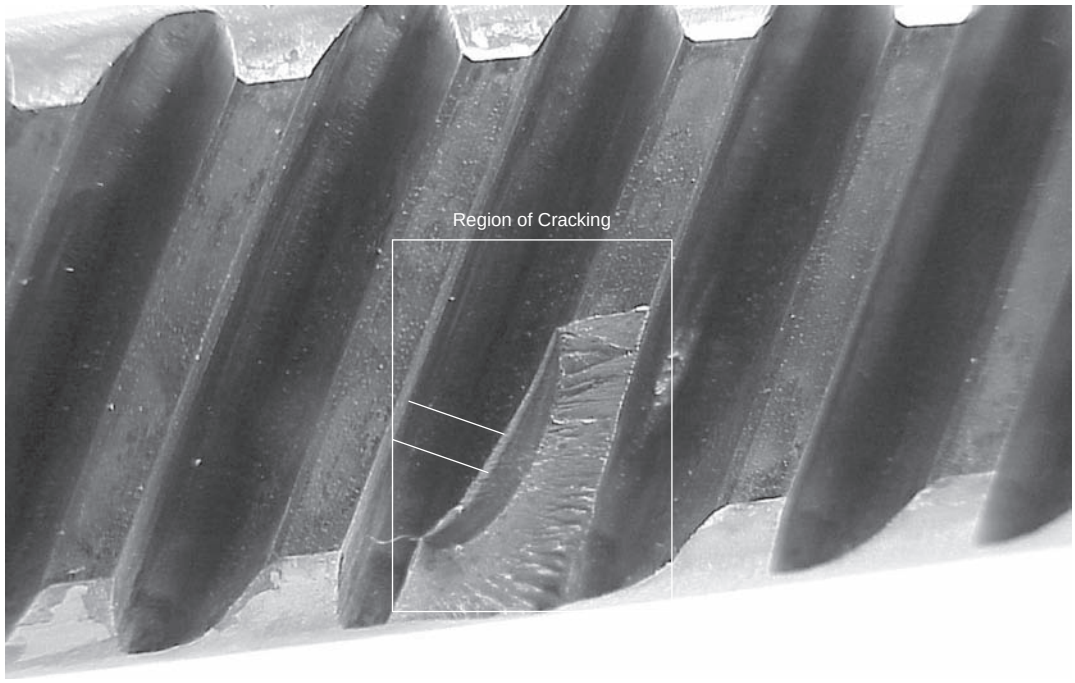

Fig. 24 Overall view of the cracked pinion showing the location of the fracture and the presence of a discolored region

Fig. 25 Closeup of the fracture region showing the discolored region. The color of the oxidation indicated that the crack occurred after quenching and during the tempering operation.

to oxidation that occurred during heat treatment. The coloration of the oxide scale suggested that the oxidation occurred during tempering (Fig. 25, 26). If the crack was preexisting prior to heat treatment, it would be darker and thicker.

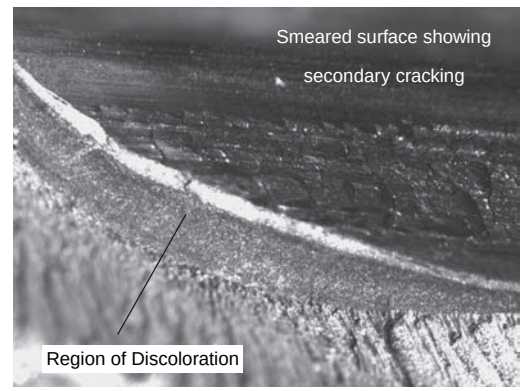

Fig. 26 Rough machining at the surface of the tooth showing smearing and tearing of the machined surface. This is suggestive of abusive machining, due to dull cutting tools, inadequate coolant, or excessive speeds and feeds.

Examination of the tooth faces showed secondary cracking at regions of tearing and smearing along the tooth face (Fig. 27), suggestive of abusive machining practice, including the use of a tool that was dull or excessive feeds and cutting speeds.

© 2008 ASM International. All Rights Reserved.
Failure Analysis of Heat Treated Steel Component (#05113G) www.asminternational.org

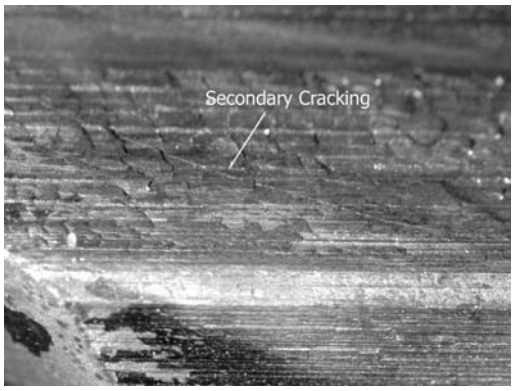

Fig. 27 Secondary cracking evident at regions of abusive machining

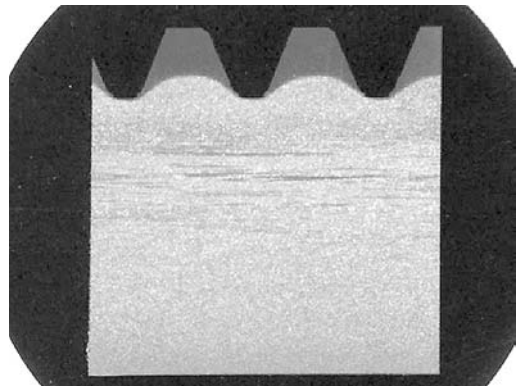

Fig. 28 Metallographic specimen of the pinion showing inadequate case at the root of the tooth. Etched in 0.5% nital

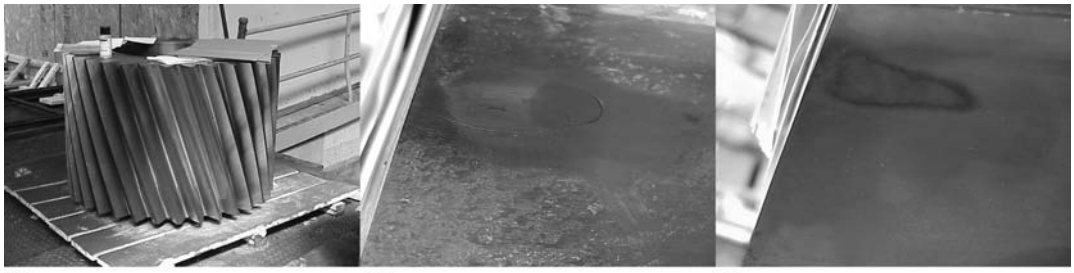

Fig. 29 Large gear that showed evidence of cracking. (a) As-received gear. (b) Crack evident on gear face. (c) Region after temper etching showing evidence of abusive grinding

Metallography of the teeth showed no evidence of burning or excessive temperature. The root of the tooth showed little evidence of proper hardening or case (Fig. 28). The microstructure in the root consisted of ferrite and pearlite, with lightly tempered martensite, further suggesting inadequate heat treatment. The tooth tip showed a fine-grained martensitic structure. No evidence of overheating was present. Examination of the tooth surface showed tears and smearing. Microhardness of the hardened regions of the tooth showed a hardness of HRC 58, while the root of the tooth was HRC 29, consistent with the observed microstructure.

Investigation of the induction heat treating conditions revealed that the concentration of the quenchant used was approximately 5%, while 6 to 10% was specified. The concentration was controlled solely by refractometer. Contamination of the quenchant was unknown.

Based on the evidence, it was determined that fracture and failure of the pinion gear tooth was caused by quench cracking, aggravated by improper concentration control and induction-hardening parameters. The situation was further aggravated by poor machining practice, creating tearing and smearing at the surface.

Often, quench cracking can result not from heat treating operations but from other sources, such as abusive grinding (Fig. 29). In this case, a large gear was found to be cracked. As is usually the case, the heat treater was blamed. Temper etching of the region of cracking showed a darkened region, suggesting overtempering of the part in a localized region.

Localized overheating during service can also result in quench cracking. A hook-point, used for catching the large cable on an aircraft carrier, showed evidence of cracking in the cable groove (Fig. 30) after a carrier landing. The hook-point was manufactured from AMS 6411 (AISI 4330V), heat treated, and a high-velocity oxy-fuel (HVOF) coating was applied. Imprints of the arresting cable were left in the cable groove.

© 2008 ASM International. All Rights Reserved.
Failure Analysis of Heat Treated Steel Component (#05113G) www.asminternational.org

The vertical cracks were exposed using liquid nitrogen and impact loading. The crack faces were discolored with a golden tint; they were subsequently examined using the SEM (Fig. 31). The cracks were intergranular along prior-austenite grains. The laboratory fracture showed microvoid coalescence. The cracks showed three distinct regions: incipient melting at the surface, intergranular regions, and laboratory-induced ductile fracture (Fig. 32).

Fig. 30 Arresting gear hook-point showing vertical cracking in the cable groove and evidence of localized heating (from the temper colors in the cable groove)

A metallographic section (Fig. 33) through the vertical cracks showed untempered martensite at the surface, a transition region of overtempered martensite, and finally, a region of tempered martensite. No evidence of the HVOF coating was observed at the crack initiation site. Hardness in the core was KHN 460. Hardness in the transition region was KHN 390, and the surface had a hardness of KHN 620. The microstructure is similar to a weldment heat-affected zone and shows that a significant heat event occurred.

Chemical analysis showed that the material conformed to AMS 6411, with alloying elements at the top of the range increasing the sensitivity to quench cracking. Hydrogen analysis indicated 0.8 ppm hydrogen. The levels of hydrogen present and the high strain rate of

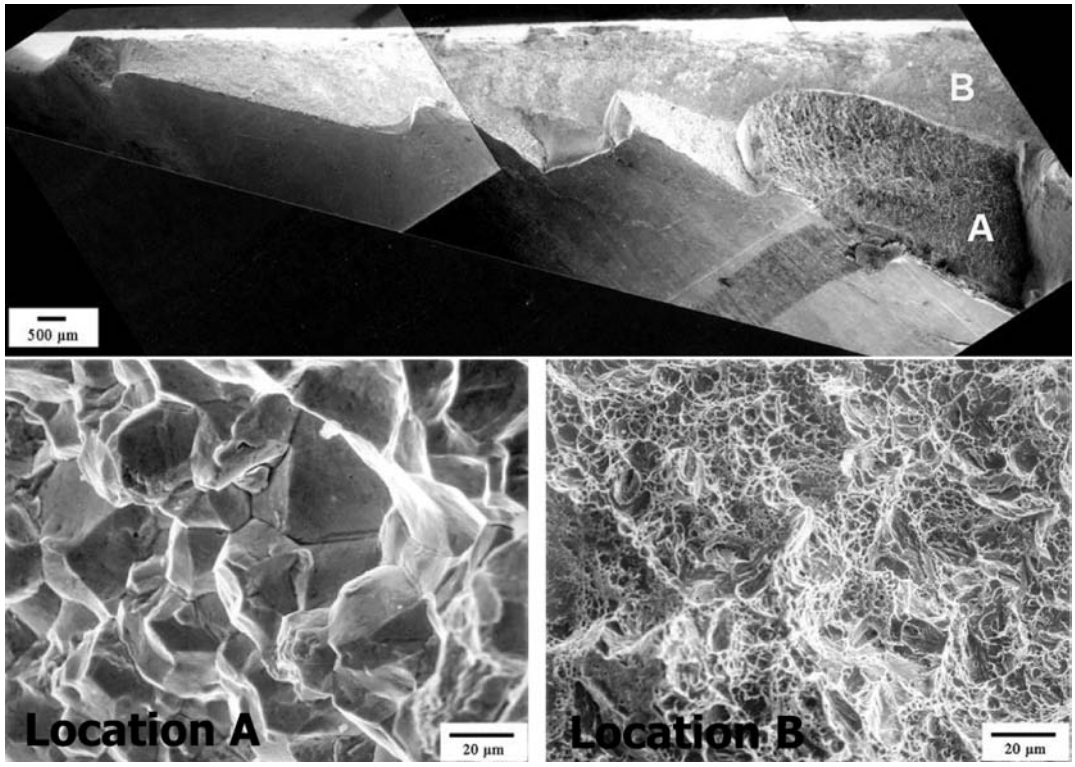

Fig. 31 SEM examination of the vertical cracking. "A" indicates the presence of intergranular cracking along prior-austenite grain boundaries. "B" indicates microvoid coalescence from the laboratory fracture during the exposure of the crack face.

© 2008 ASM International. All Rights Reserved.
Failure Analysis of Heat Treated Steel Component (#05113G) www.asminternational.org

loading precludes hydrogen embrittlement as a possible failure mechanism.

Based on the analysis, it was determined that the vertical cracking in the cable groove was the result of transformational stresses from frictional heating during capture of the arresting cable by the hook-point. The mechanism is similar to quench cracking and was aggravated

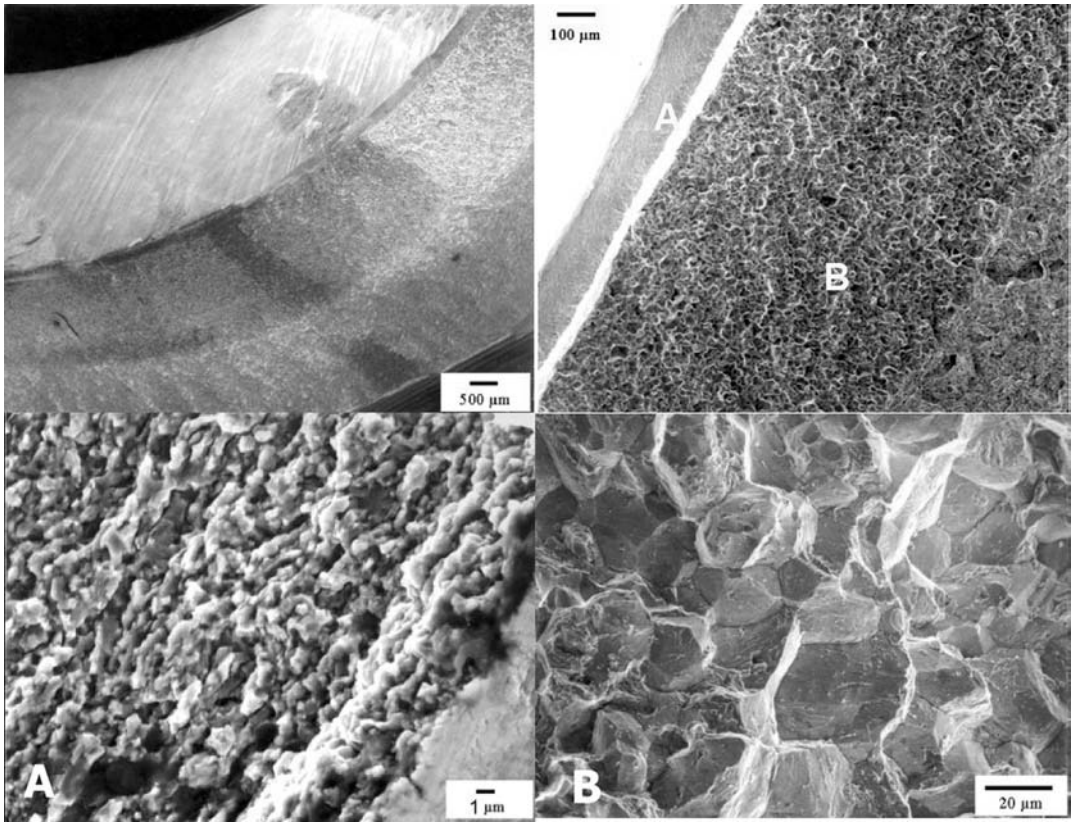

Fig. 32 Exposed crack face showing two distinct regions on the crack face. "A," region of incipient melting. "B," intergranular fracture

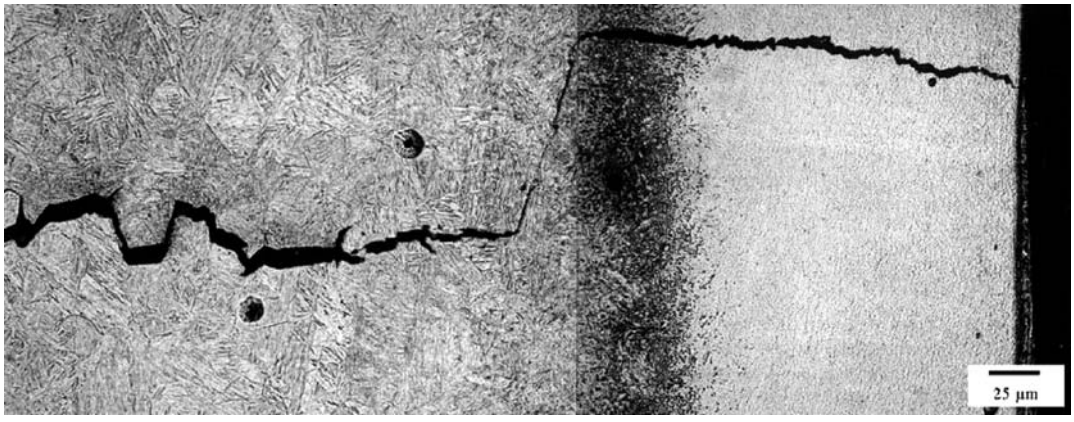

Fig. 33 Metallographic section through the vertical crack showing (from right to left) a lightly etching region of fine-grained untempered martensite, a transition region of overtempered martensite, and a region of nominally tempered martensite. Hardness in the untempered martensite was KHN 620. The transition region showed a hardness of 390 KHN, and the nominal core hardness was KHN 460

© 2008 ASM International. All Rights Reserved.
Failure Analysis of Heat Treated Steel Component (#05113G) www.asminternational.org

by the higher-than-normal hardenability of the alloy. Recommendations included the application of a different HVOF coating to better resist the frictional heating of the cable during carrier arrestments.

Tempered martensite embrittlement (TME) may not be associated with impurity atoms segregating to prior-austenite grain boundaries. The most common factor in TME is the formation of cementite during tempering (Ref 35). When a given steel has a low impurity content, the source of TME is the decomposition of retained austenite during the second stage of tempering. Thomas first proposed this mechanism (Ref 36). This was found when transmission electron microscopy showed the presence of thin regions of retained austenite between martensite in as-quenched steels, which subsequently transformed to cementite on tempering in the range of 230 to 470 °C (450 to 700 °F).

The presence of phosphorus also plays a role. If two steels are compared, one containing a higher concentration of phosphorus, the steel with the higher phosphorus content will have poorer impact properties than an identical steel with a lower phosphorus level. This will remain true through the entire range of tempering temperature up to approximately 500 °C (932 °F). The fracture mode is intergranular along prior-austenite grain boundaries (Ref 37). It is likely that phosphorus is present at the prior-austenite grain boundaries. It is only after cementite precipitates in the tempered martensite that TME is fully present. Often, the presence of molybdenum at concentrations up to approximately 0.5% will reduce the effect of TME.

On June 19, 1974, during a cold start after a long shutdown for repairing the Tennessee Valley Authority Gallatin No. 2 unit, the intermediate-pressure/low-pressure rotor burst at approximately 3400 rpm. The rotor had been in operation for 106,000 h from its operational start in May 1957 (Ref 38). The burst rotor was forged from an air-melted ingot. This ingot was produced by a large region of MnS segregation zone that was present at the center of the ingot, which was subsequently bored by machining during fabrication of the rotor. The steam temperature was 566 °C (1050 °F). Tempered martensite embrittlement occurred over the long period of operation and substantially reduced the toughness of the rotor. The presence of the MnS inclusions initiated fracture by creep-fatigue interaction and was enhanced by the presence of TME (Ref 39).

Rail steels have been documented to fail because of TME (Ref 40). This was especially true of older rails manufactured in open-hearth furnaces with high phosphorus content. This occurred because of slow cooling through the 500 °C (930 °F) range or from isothermal holding at 500 °C. Figure 34 shows a representative SEM fractograph of an Fe-0.26C-2.11Si-2.27Mn-1.59Cr wt% carbide-free bainitic rail steel that has been temper embrittled by heat treatment at 500 °C for 5 h (Ref 40).

Temper embrittlement is only now becoming understood with regard to its mechanism. However, the conditions of temper embrittlement are well known (Ref 41, 42).

Steels must be heat treated or cooled through the range of 375 to 575 °C (706 to 1070 °F) in order to become temper embrittled. Temper embrittlement is typically detected by an increase in the ductile-to-brittle transition temperature. This is shown in Fig. 35 for AISI 3140 steel temper embrittled by furnace cooling through the critical range and holding at 550 °C (1020 °F) (Ref 35). The embrittlement reaction follows a typical C-curve, with the minimum in embrittling time at approximately 1 h at 550 °C (1020 °F) and several hundred hours at 375 °C (706 °F) (Ref 43). By heating to approximately 575 °C (1070 °F), temper embrittlement is reversible and can be eliminated after holding for only a few minutes at temperature.

For temper embrittlement to occur, specific embrittling impurities must be present. These include antimony, phosphorus, tin, and arsenic. Quantities of less than 0.01% are enough to cause temper embrittlement. For the most part, simple plain carbon steels are not considered to be susceptible to temper embrittlement

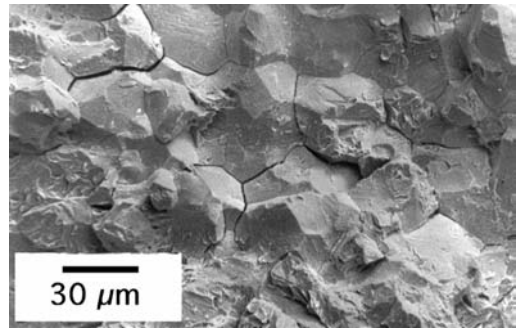

Fig. 34 SEM fractograph of Fe-0.26C-2.11Si-2.27Mn-1.59Cr wt% carbide-free bainitic rail steel that has been temper embrittled by heat treatment at 500 °C for 5 h

© 2008 ASM International. All Rights Reserved.
Failure Analysis of Heat Treated Steel Component (#05113G) www.asminternational.org

as long as manganese concentrations are held to below 0.5%. Alloy steels containing chromium and nickel are the most prone; however, additions of molybdenum at a concentration of up to 0.5% are effective in reducing the susceptibility of these steels to temper embrittlement.

Large forgings have been prone to temper embrittlement because of the slow cooling that occurs during fabrication. These large forgings are also prone because of the operating temperatures applied, especially in large turbine rotors.

Liquid Metal Embrittlement or Solid Metal Embrittlement. Exposure of steels to liquid metals has been observed to result in brittle fracture along prior-austenite grain boundaries (Ref 44). Steels may be embrittled by exposure to any of the low-melting metals shown in Table 1 (Ref 45). Embrittlement occurs by wetting of the prior-austenite grain boundaries with a thin film of the molten metal. Usually, very low tensile stresses are required to fail parts that are liquid metal embrittled.

In general, three conditions are necessary for liquid metal embrittlement. First, the embrittling metal must be present, either externally as a coating or internally. Internal sources can include lead used to enhance machinability. Second, temperatures that the part is exposed to must be high enough that the embrittling metal can melt. Lastly, tensile stresses must be present as externally applied or internal residual stresses. Should any of these conditions not be met, then it is unlikely that the steel will fail by liquid metal embrittlement.

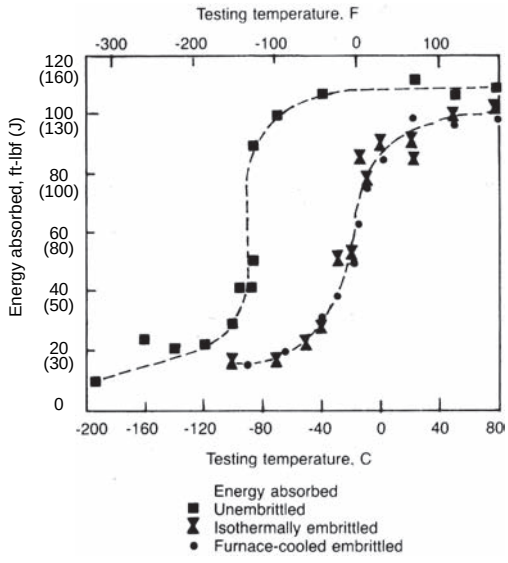

Fig. 35 Shift in ductile-brittle transition temperature curve to a higher temperature for AISI 3140 steel by holding at 500 °C and continuous cooling through the temper embrittlement critical range. Source: Ref 35

Liquid metal embrittlement has been known to embrittle gun tubes. In 1977, during the manufacture of a 105 mm M68 gun tube, lead was electroplated to the tube and used as a lubricant during the autofrettage process. During the postautofrettage thermal treatment, the lead melted and embrittled the gun tube. A complete transverse brittle failure occurred. The axial tensile residual stresses from the autofrettage process were adequate to completely fracture the tube, even though the hoop stresses were much greater (Ref 46).

In another example, an ISO 8.8 low-alloy steel bolt that was electroplated with cadmium was used for an extended time at an elevated temperature of 230 °C (455 °F). The resulting failure showed intergranular fracture, with cadmium penetration along grain boundaries. This cadmium penetration was detected by x-ray diffraction (Fig. 36) (Ref 9).

On April 28, 1997, United Flight 1210, a Boeing 737–222 equipped with Pratt and Whitney JT8D-7B engines, experienced an uncontained failure of the No. 2 engine (right side, facing forward) high-pressure compressor stage disk during takeoff. Takeoff was aborted, and the aircraft was evacuated. Only two passengers were slightly injured during evacuation. Postincident examination of the engine revealed that two-fragments (approximately 50 by 100 mm, or 2 by 4 in.) separated from the disk. Examination of the disk revealed a 100 mm (4 in.) circumferential fracture around the diameter, with three additional fractures emanating diagonally outward toward the rim. Also, cracks

Table 1 Melting temperatures of metals known to embrittle high-strength steels

Metal	Melting temperature °C	°F
Mercury	−39	−38
Gallium	29	85
Indium	156	313
Lithium	180	356
Cadmium	321	610
Tin	232	449
Lead	327	620
Zinc	419	787
Antimony	642	1187

Source: Ref 45

© 2008 ASM International. All Rights Reserved.
Failure Analysis of Heat Treated Steel Component (#05113G) www.asminternational.org

emanated radially outward from two tie-rod holes, one of which bisected the fracture at the diameter. No cracks were detected on any of the other high-pressure compressor disks in the engine.

On further examination by the National Transportation Safety Board, the fractures were found to have large intergranular areas in the steel compressor disk (Ref 47). Solid molten cadmium was detected along the prior-austenite grain boundaries, indicative of liquid metal (cadmium) embrittlement. Inadequate nickel plating prestrike thickness was observed at the surface of the disk. The failed disk was plated by a trainee and inadequately plated with nickel. It was found that the nickel plating was approximately 0.003 mm (0.00012 in.) in thickness, which is below the Pratt and Whitney specified thickness of 0.015 to 0.02 mm (0.0006 to 0.0008 in.). This thickness was inadequate to prevent migration of cadmium into the steel grain boundaries.

This was not the first time that liquid metal embrittlement occurred in a compressor disk. On July 23, 1990, the crew of a JT8D-9-equipped Boeing 737–100 reported that they heard a muffled explosion during climb, followed by a loss of rpm of the No. 1 (left) engine. The crew returned to Houston, Texas, without incident. Engine examination revealed a failure of a disk spacer due to liquid metal embrittlement (Ref 48).

An AISI 4330V hook-point failed during field trials. This hook-point is used to grab the cable on aircraft carriers and arrest the forward movement of the aircraft during landing. Previous hook-points failed because of excessive hardness and high triaxial stresses during impact loading. These hook-points were evaluated, and discrepant parts were segregated. A series of parts were then retempered to the specified hardness of HRC 46 from HRC 51. The lug radius was enlarged, and a new HVOF coating was applied. During field trials, multiple hook-points were identified by magnetic particle inspection as having cracks in the lug radius (Fig. 37). No through cracks were found. The cracks were exposed, and a narrow uniform region of intergranular fracture (approximately 200 μm) was observed (Fig. 38). Metallography indicated that the microstructure was quenched and tempered martensite, and the hardness was within the specification of 46 to 48 HRC. Metallography revealed that no decarburization or precipitates were found at the prior-austenite grain boundaries. Hydrogen analysis showed a concentration of 0.2 ppm of hydrogen. The low concentration of hydrogen and the rapid rate of loading eliminated hydrogen embrittlement as a cause of cracking. Auger analysis of the grain boundaries within the intergranular region showed the presence of cadmium at the grain boundaries. The concentration of cadmium also decreased as the grain boundaries were ion milled away. This analysis indicated that the fracture occurred because of liquid metal embrittlement or solid metal embrittlement. Solid metal embrittlement is similar to liquid metal embrittlement, except that temperatures are not high enough to cause melting of the cadmium. For cadmium, solid metal embrittlement can occur at temperatures above 230 °C (450 °F). A review of the planning showed that the work order release did not include removal of the cadmium plating prior to retempering of the hook-points. Tempering to bring the hook-points to the proper hardness was above 320 °C (610 °F). Based on this, it was determined that

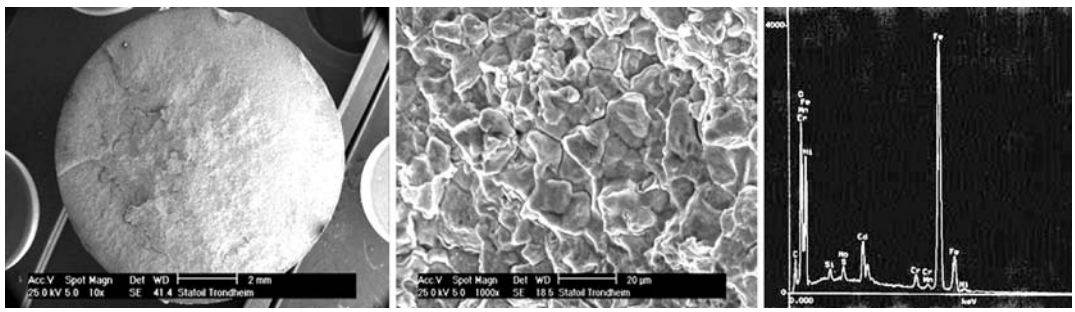

Fig. 36 Liquid metal embrittlement of a low-alloy bolt plated with cadmium that failed during service. Cadmium was found to have penetrated at the grain boundaries due to service above 230 °C. (a) Overall fracture surface. (b) SEM examination of fracture showing intergranular fracture. (c) X-ray diffraction spectrum at grain boundaries showing cadmium penetration

© 2008 ASM International. All Rights Reserved.
Failure Analysis of Heat Treated Steel Component (#05113G) www.asminternational.org

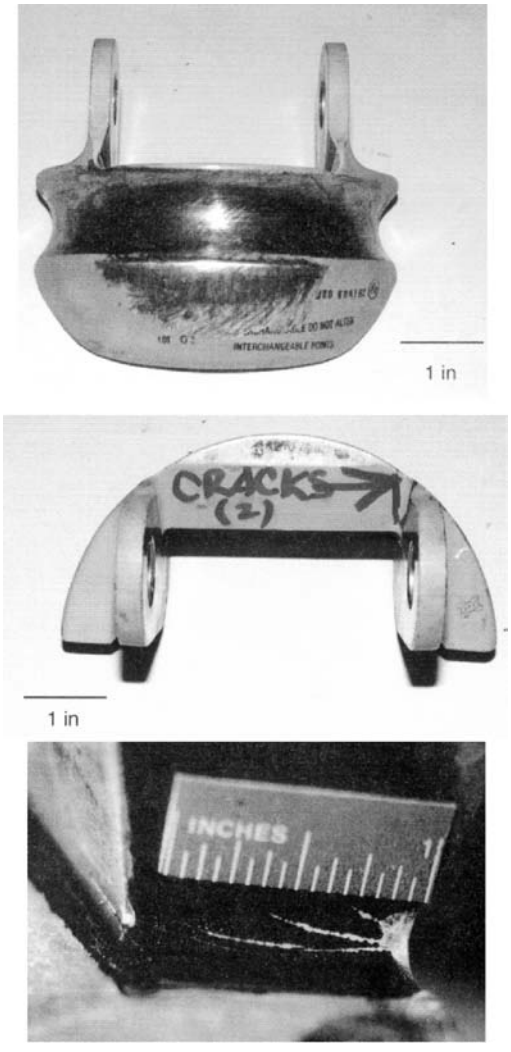

Fig. 37 AISI 4330V cadmium-plated hook-point used to arrest landings of naval aircraft. Overall view of the part, showing location of cracks observed using nondestructive testing

the cracking observed in the hook-points was due to liquid metal embrittlement caused by failure to remove the cadmium plating prior to tempering.

Hydrogen embrittlement is a particularly insidious form of failure. Often, failure is delayed for hours, months, and possibly years after the component has been fabricated. The results may be catastrophic and unpredictable. The failure mode is typically intergranular along prior-austenite grain boundaries (Fig. 21).

Hydrogen can come from either external or internal sources. One common source of hydrogen is the steelmaking process (Ref 49), and it is a significant problem in large sections (Ref 50), where hydrogen embrittlement is observed as flakes or a reduction in ductility (Ref 51). These flakes or blisters are regions where hydrogen collects, until a bubble of hydrogen is adequate to deform the surrounding region.

External sources of hydrogen are from manufacturing processes such as pickling (Ref 52, 53) and plating (Ref 54–56). Additional sources of hydrogen can be the result of galvanic coupling in an aqueous medium, in a similar fashion to electroplating.

One of the particularly serious characteristics of hydrogen embrittlement is the incubation time required for it to occur. As a general rule, the higher the hydrogen concentration, the shorter the time to failure. For a given hydrogen concentration, as the stress is increased, the incubation time is decreased.

In quenched and tempered steels, there are a number of sites that can trap hydrogen. These include martensite interlath interfaces, high density of dislocations, and the carbide-matrix interface. All of these sites can act as traps for hydrogen (Ref 57). Once present, hydrogen diffuses to traps, such as dislocation cores, and is transported by dislocation motion (Ref 58). Hydrogen can also collect at inclusions and carbides, which are also good hydrogen traps. The incubation time is dependent on the hydrogen diffusion rate in steel to the point of crack initiation.

Quenched and tempered steels that have a hardness above HRC 38 are generally given a hydrogen embrittlement relief at 135 °C (275 °F) for 24 h. This enables the hydrogen in the part to diffuse out. This is based on the study by Johnson, Morlet, and Troiano (Fig. 39) (Ref 59). This hydrogen embrittlement relief is usually mandated whenever parts are plated, cleaned, or exposed in some fashion to aqueous solutions such as coolants or acid. Alkaline solutions are not generally prone to causing hydrogen embrittlement.

Fasteners are prone to hydrogen embrittlement. In this example, an ISO 10.9 low-alloy steel bolt grade that was zinc plated failed during service. Multiple fracture initiation sites were evident along the bolt head transition, with intergranular fracture morphology and heavy secondary cracking. A hydrogen source was suggested from manufacturing (pickling stage) and/or cathodic hydrogen charging due to anodic zinc plating (Fig. 40) (Ref 9).

© 2008 ASM International. All Rights Reserved.
Failure Analysis of Heat Treated Steel Component (#05113G) www.asminternational.org

To verify that the baking process after chromium plating was adequate, a plating shop tested four chromium-plated 4340 notched tensile specimens. These test specimens were heat treated to 1515 MPa (220 ksi) and chromium plated. During a sustained load test, one of the

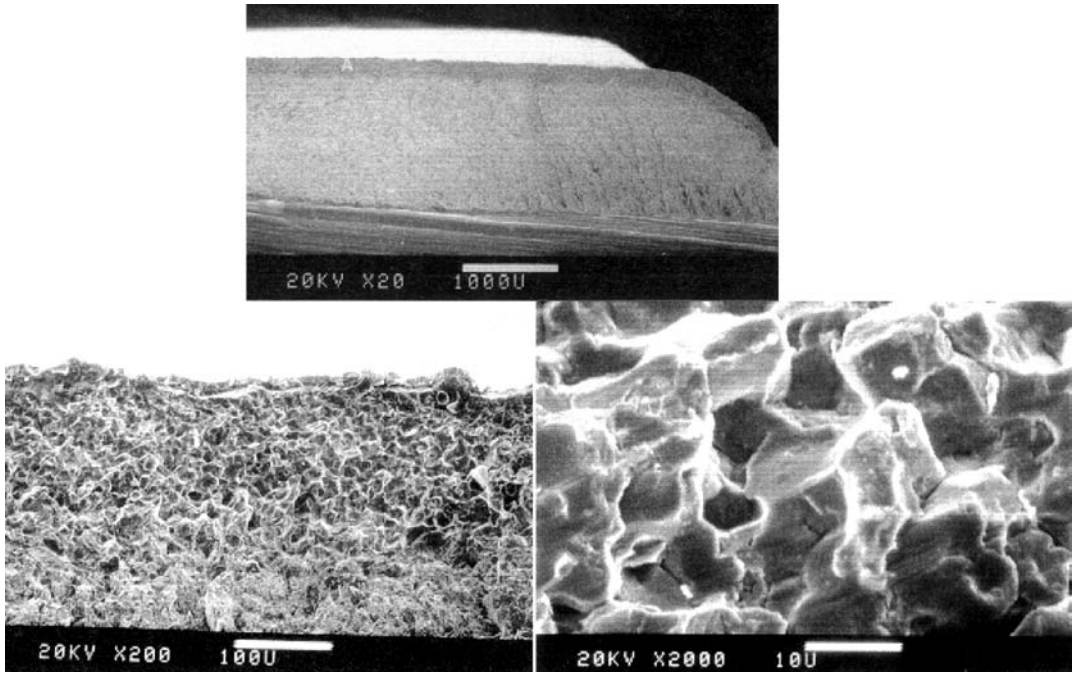

Fig. 38 SEM examination of the hook-point showing a narrow region of intergranular fracture along prior-austenite grain boundaries

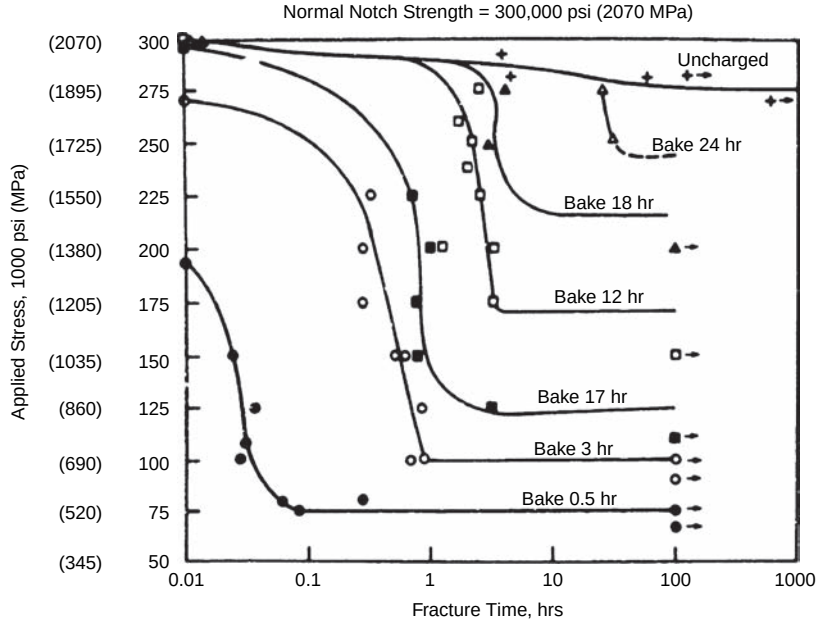

Fig. 39 Baking AISI 4340 steel at 300 °F for different times, showing the effect of baking on the incubation of failure

© 2008 ASM International. All Rights Reserved.
Failure Analysis of Heat Treated Steel Component (#05113G) www.asminternational.org

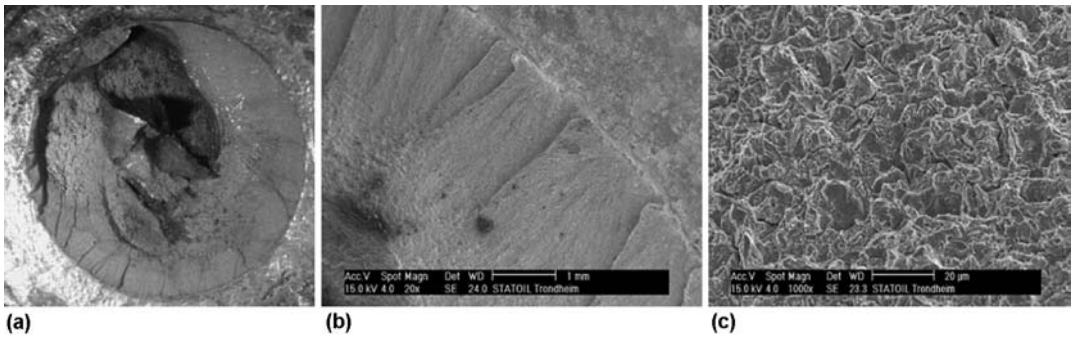

Fig. 40 Hydrogen embrittlement failure of an ISO 10.9 low-alloy steel bolt grade. (a) As-received bolt. (b) Multiple initiation sites with secondary cracks evident. (c) Intergranular fracture along prior-austenite grain boundaries

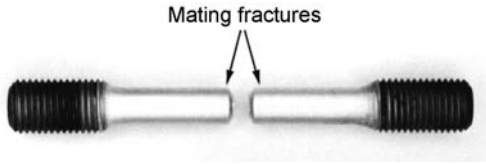

Fig. 41 As-received notched tensile specimen showing location of fracture. Tensile specimen was fabricated from 4340 steel, heat treated to 1515 MPa (220 ksi), and chromium plated.

specimens failed prematurely (Fig. 41). The fracture was located at the notch. The fracture surface (Fig. 42) was examined, and the origin showed a shiny, faceted surface. At the origin, the fracture was intergranular, while away from the origin, near the center of the fracture surface, the fracture mechanism was microvoid coalescence. Hydrogen analysis on the notched tensile specimen yielded an average hydrogen concentration of 12 ppm hydrogen. This is considered very high and is sufficient to cause hydrogen embrittlement. Metallography of the test specimen showed a normal quenched and tempered microstructure, typical of a steel heat treated to this hardness.

During a routine wheel and tire change, a new jack pad for a military aircraft failed, causing an aircraft to drop prematurely onto the new wheel. No damage occurred to the aircraft. The jack pad was machined from 300M steel that was heat treated to HRC 54 to 55. The jack pad was chromium plated.

The as-received jack pad (Fig. 43) was examined, and two fracture surfaces were identified (Fig. 44). These were identified as origins 1 and 2. Ridges emanated away from a distinct origin location on each of the fracture surfaces. Evidence of light corrosion products was found at the fracture origin of origin 2. SEM examination of each of the origins (Fig. 45, 46) revealed that the fracture was intergranular. At a distance away from the origin, the fracture consisted of microvoid coalescence, consistent with rapid ductile rupture.

A metallographic specimen was removed from the largest origin location and examined (Fig. 47). The microstructure of the steel was quenched and tempered martensite, typical of 300M heat treated to HRC 54 to 55. Chromium plating was found to be intact at the fracture origin.

Hydrogen analysis conducted on the jack pad showed hydrogen concentrations of 4 and 6 ppm, which is considered adequate hydrogen to cause hydrogen embrittlement in 300M steel heat treated to this hardness.

Based on this investigation, it was concluded that the jack pad most likely failed from hydrogen embrittlement.

Stress-corrosion cracking is the attack of a material by the combined action of tensile stress on a part, either externally from an applied force or internally from residual stresses, and a specific corrosive environment. Common features are brittle fracture with little ductility, localized corrosive attack, and a specific environmental-alloy system. Failure by stress-corrosion cracking (SCC) is characterized by exposure to a specific chemical environment and the simultaneous application of a tensile stress. Without one or the other, SCC will not occur. Fine cracks can penetrate deeply into the part without obvious signs of attack. Impending failure can occur without warning.

The applied tensile stresses can be from the service environment or from any of the

© 2008 ASM International. All Rights Reserved.
Failure Analysis of Heat Treated Steel Component (#05113G) www.asminternational.org

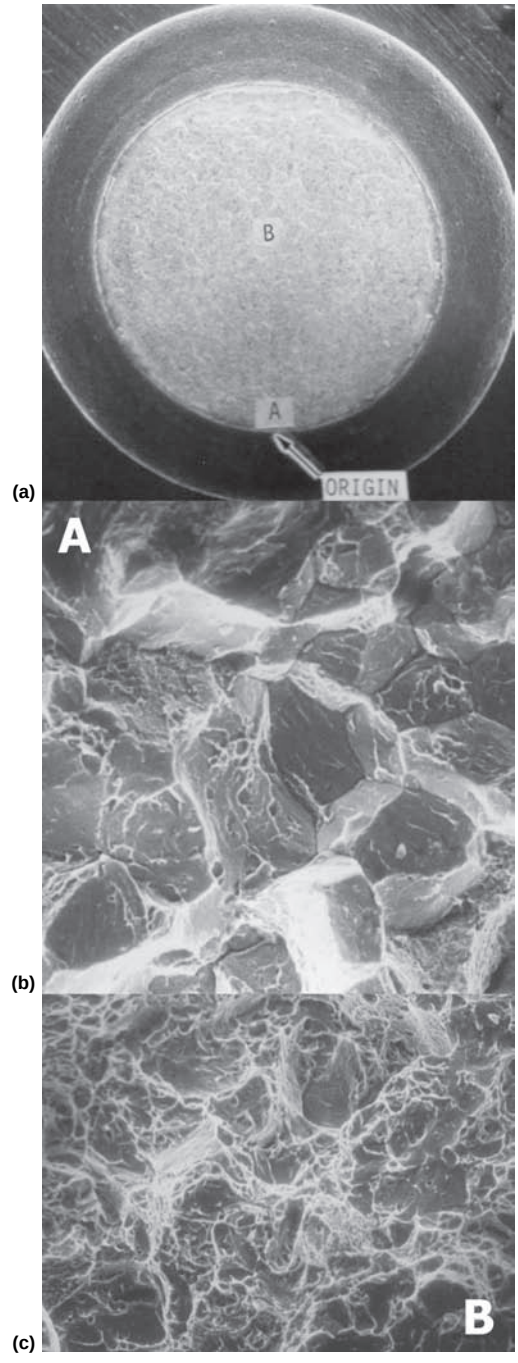

Fig. 42 Overall view of the fracture surface, showing location and results of SEM examinations. (a) Overall fracture surface and location of origin. (b) Intergranular fracture at the origin of cracking (location A). Original magnification: 1000×. (b) Microvoid coalescence at location B

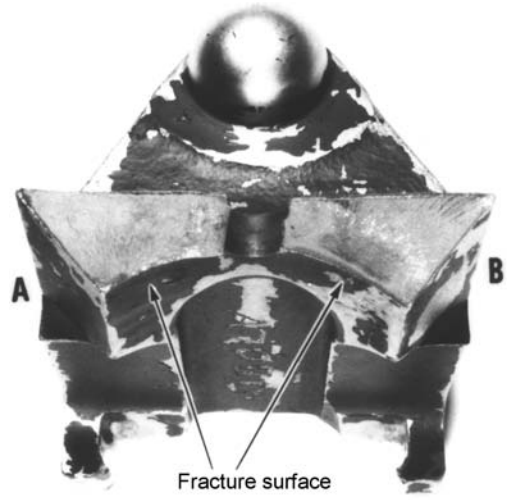

Fig. 43 As-received jack pad showing the locations of the two distinct origins on the inside bore of the hole for a pressed-in pin

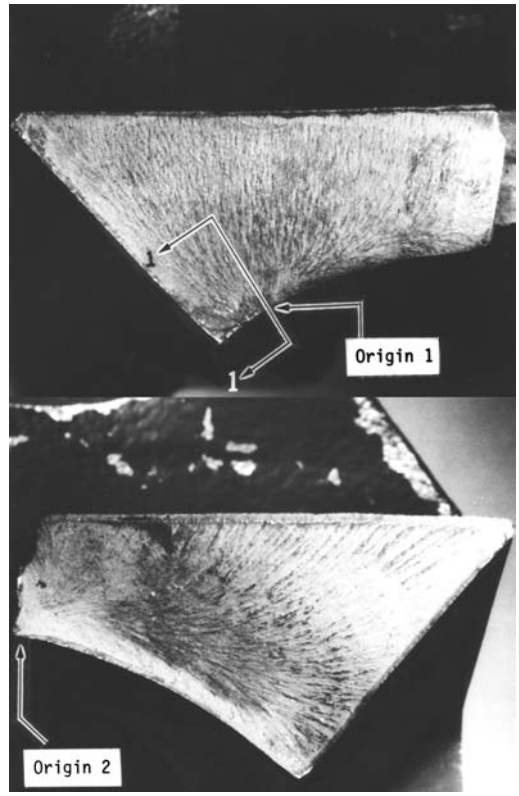

Fig. 44 Fracture surfaces of the jack pad showing location of the origins. Original magnification: 2×

© 2008 ASM International. All Rights Reserved.
Failure Analysis of Heat Treated Steel Component (#05113G) www.asminternational.org

numerous sources of residual stresses from manufacturing (thermal processing, machining, grinding, surface finishing, fabrication, or assembly). The tensile stress is important in the rupture of any protective film during initiation and subsequent propagation of the crack. There appears to be a threshold tensile stress intensity, K_{ISCC}, below which SCC does not occur. This stress intensity is dependent on the alloy, the heat treated condition, and the environment.

The site of initiation of SCC may be microscopic. This could be from local differences in metal composition or stress concentrations. A pre-existing mechanical flaw or discontinuity may act as a stress raiser and serve as a site for SCC initiation.

Stress corrosion cracking usually exhibits extensive branching and propagates in a direction

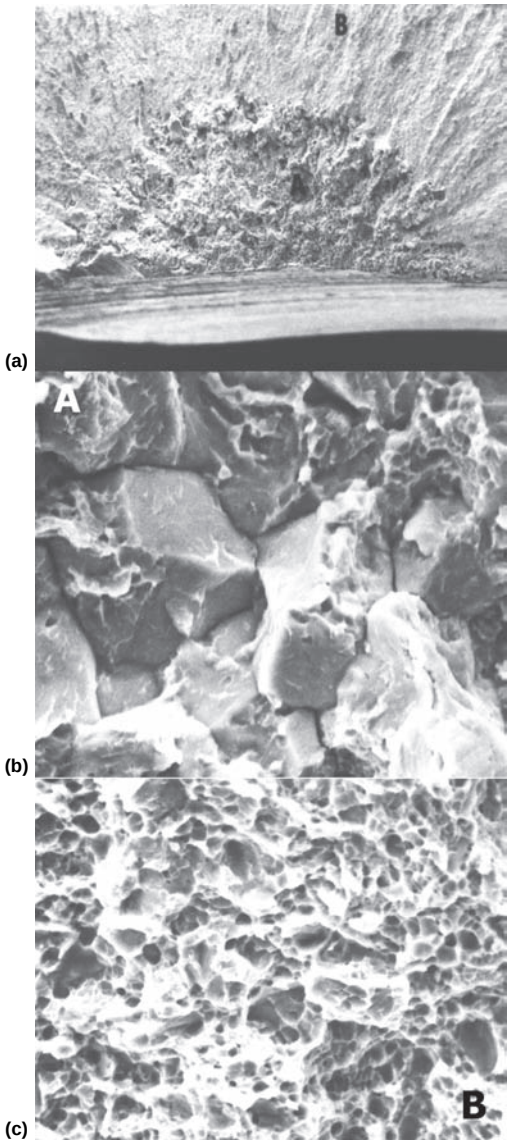

Fig. 45 SEM examination of origin 1. (a) Location of the fracture origin. Original magnification: 20×. (b) Location A showing a region of intergranular fracture along prior-austenite grain boundaries. Original magnification: 1000×. (c) Location B, at a distance away from origin 1, showing microvoid coalescence. Original magnification: 2000×

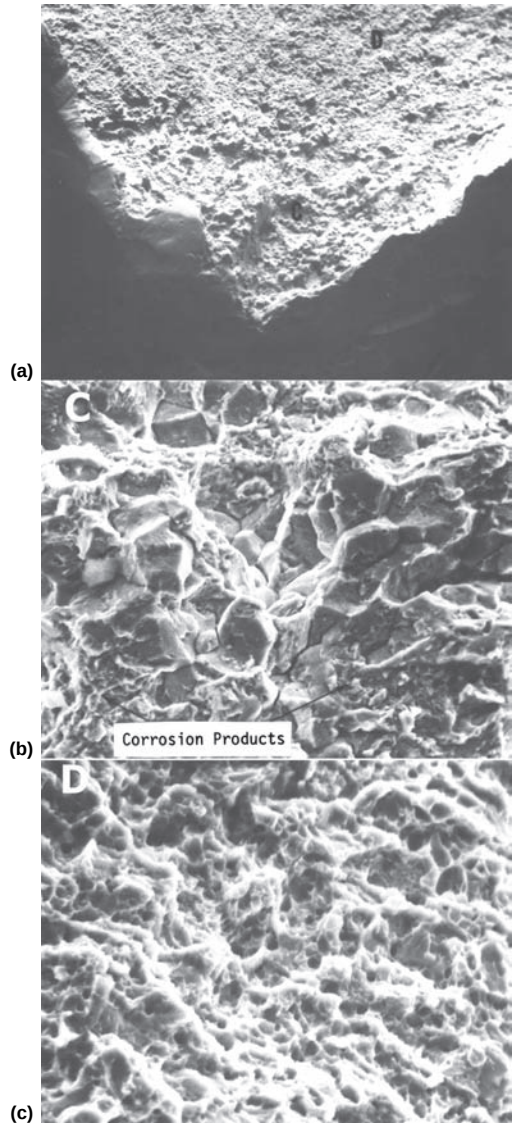

Fig. 46 SEM examination of origin 2. (a) Location of the fracture origin. Original magnification: 100×. (b) Location C showing a region of intergranular fracture along prior-austenite grain boundaries. Original magnification: 1000×. (c) Location D, at a distance away from origin 2, showing microvoid coalescence. Original magnification: 2000×

© 2008 ASM International. All Rights Reserved.
Failure Analysis of Heat Treated Steel Component (#05113G) www.asminternational.org

perpendicular to the tensile stresses contributing to propagation and initiation. However, this is not always the case. Structural steels exposed to agricultural ammonia may exhibit nonbranched cracking.

Stress-corrosion cracking has several special characteristics that differentiate it from other forms of cracking:

- Only certain specific environments for a specific alloy system cause SCC. There is no general pattern regarding the corroding environments or alloy systems.
- Pure metals are much less susceptible to SCC.
- Cathodic protection has been successful in preventing the initiation of SCC or in stopping the propagation of SCC.
- Addition of certain soluble salts effectively can "poison" the environment and either reduce or stop the propagation of SCC cracks.
- Certain metallurgical features, such as grain size, can influence the susceptibility of an alloy system to SCC attack.

Macroscopically, fractures produced by SCC show little ductility and nearly always appear brittle. The fracture surfaces usually contain regions that are identifiable as the crack initiation site, slow crack propagation, and final failure. The regions containing the slow propagation often contain corrosion products or are discolored. This region extends to the region of final fast fracture. However, this can also be misleading, because the fracture could have corroded before inspection, or the environment may not be conducive to straining the fracture.

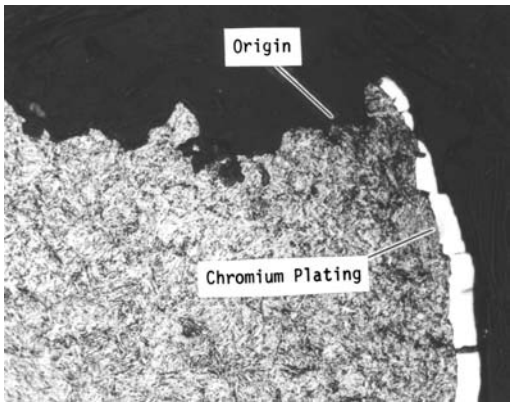

Fig. 47 Micrograph showing quenched and tempered martensite, typical of 300M heat treated to HRC 54 to 55. Note that the chromium plating is intact.

It is often difficult to differentiate between SCC and hydrogen-induced damage solely from the fracture surface. Fractures of both types exhibit intergranular features and tend to follow prior-austenite grain boundaries. Metallography is important to determine if branched cracking has occurred. Even so, the absence of branched cracking may not preclude SCC. In general, the environment that the part was exposed to can be the deciding factor of whether it is SCC or hydrogen embrittlement (Fig. 48).

Low-carbon steels generally become more susceptible to SCC as the carbon concentration increases. Decarburized steels and pure iron are resistant to SCC. Microstructure plays a greater role in susceptibility to SCC than does the alloying elements. High-alloy steels in a variety of environments show that the heat treated strength of the alloy is more important than strictly the concentration. Steels that have been heat treated to 1240 MPa (180 ksi) or higher are especially susceptible to SCC. Typical environments that can cause SCC in steels are shown in Table 2.

Caustic cracking in boilers is a serious SCC problem and has caused many failures in steam boilers. These failures usually initiate in riveted and welded structures, where small leaks allow buildup of caustic soda and silica. Cracking is usually intergranular. Failures of this type have occurred with concentrations of NaOH as low as 5% in water. Failures take place when the operating temperature is in the range of 200 to 250 °C (390 to 480 °F). The concentration of NaOH needed to cause cracking initiation decreases as the temperature is increased.

Cracking of low-carbon steels and low-alloy steels in nitrate solutions occurs in tubing and couplings in high-pressure condensate wells. Cracking in nitrate solutions is intergranular, following prior-austenite grain boundaries. Generally, acidic solutions cause this type of cracking. Raising the pH of the solution enhances resistance to SCC, while increasing the concentration of nitrate-containing solutions tends to increase the susceptibility to SCC.

Carbon steel tanks containing ammonia have also developed leaks because of SCC. Both plain carbon steels and quenched and tempered steel plate have shown a susceptibility to SCC in ammonia. Failures occurred in ammonia mixed with air and carbon dioxide. The presence of water vapor delayed cracking.

Halide-containing environments, such as seawater, are particularly severe for alloy steels

© 2008 ASM International. All Rights Reserved.
Failure Analysis of Heat Treated Steel Component (#05113G) www.asminternational.org

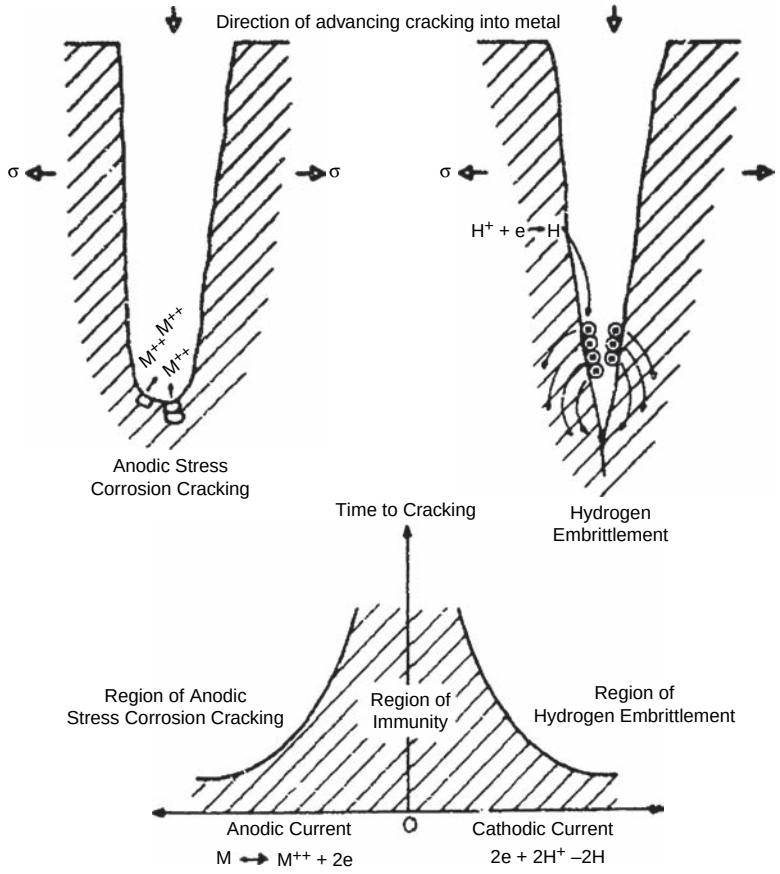

Fig. 48 Schematic differentiation of anodic stress-corrosion cracking and cathodic hydrogen embrittlement

Table 2 Environments that produce stress-corrosion failures in carbon and low-alloy steels

Medium	Type of fracture (a)	Comments
Aqueous chloride environments	I,T	Prevalent in high-strength steels heat treated to 1380 MPa (200 ksi) or greater
Caustic solutions	I	Well known as caustic embrittlement
Nitrates	I	Examples of bridge cable failures in ammonium nitrate or sodium nitrate solutions
HNO_3	I	. . .
HCN	I	. . .
Seacoast and industrial environments	I	High-strength steels heat treated to 1380 MPa (200 ksi) or greater are especially prone.
Water, humid air, and gas	I	High-strength steels heat treated to 1380 MPa (200 ksi) or greater are especially prone.

(a) I, intergranular failure; T, transgranular failure

heat treated to above 1380 MPa (200 ksi). The use of cadmium plating, low-hydrogen practices, and adequate baking are helpful in preventing SCC in steels such as 300M or 4340.

On August 22, 2003, an empty cargo tanker pulled upto a tank containing anhydrous ammonia. Approximately 1 hour after being filled, the front head cracked open (Fig. 49) and started to release anhydrous ammonia. Approximately 100 workers were evacuated from the building. Five people were treated for inhalation injuries and released. The cost to repair the trailer was approximately $25,000.

Examination revealed a 40 cm (16 in.) long through-wall crack next to the radial weld in the front head at the 1 o'clock position (Fig. 50). Internal examination using magnetic particle inspection found two additional cracks that had not yet propagated through the wall of the tanker. SEM examination of the cracks (Ref 60) found that the fracture was branched and intergranular, with extensive surface corrosion on the crack faces.

© 2008 ASM International. All Rights Reserved.

In the 1950s, the Agricultural Ammonia Institute determined that caustic cracking of ammonia-containing tanks was the reason that a number of carbon steel tanks had failed (Ref 61). They further determined that the addition of 0.1% water to anhydrous ammonia inhibited SCC in carbon steel. The committee recommended that at least 0.2% water be added to inhibit cracking. Further cracking occurred in the 1960s in quenched and tempered ASTM A517 steel, because purity levels had increased and water was no longer being added. In 1975, the Department of Transportation adopted regulations (Title 49 Code of Federal Regulations, Parts 171 to 180) that required cargo tanks fabricated from quenched and tempered steel should only be used for anhydrous ammonia if the solution contained 0.2% water. The regulation further required tankers to be placarded with signs indicating "QT" or "NQT," for quenched and tempered or not quenched and tempered.

The National Transportation Safety Board determined that the failure of the tank and the subsequent release of anhydrous ammonia were due to caustic cracking (SCC) of the tank from the transport of anhydrous ammonia containing less than 0.2% water.

A Boeing 757–2008 was parked at a gate at Copenhagen, Denmark, and boarding of passengers was nearly completed when the right-hand main landing gear truck beam failed (Ref 62). As the beam failed, the right side of the aircraft rested on the shock strut instead of on the wheels. Figure 51 shows the failed truck beam and the aircraft resting on the shock strut. A

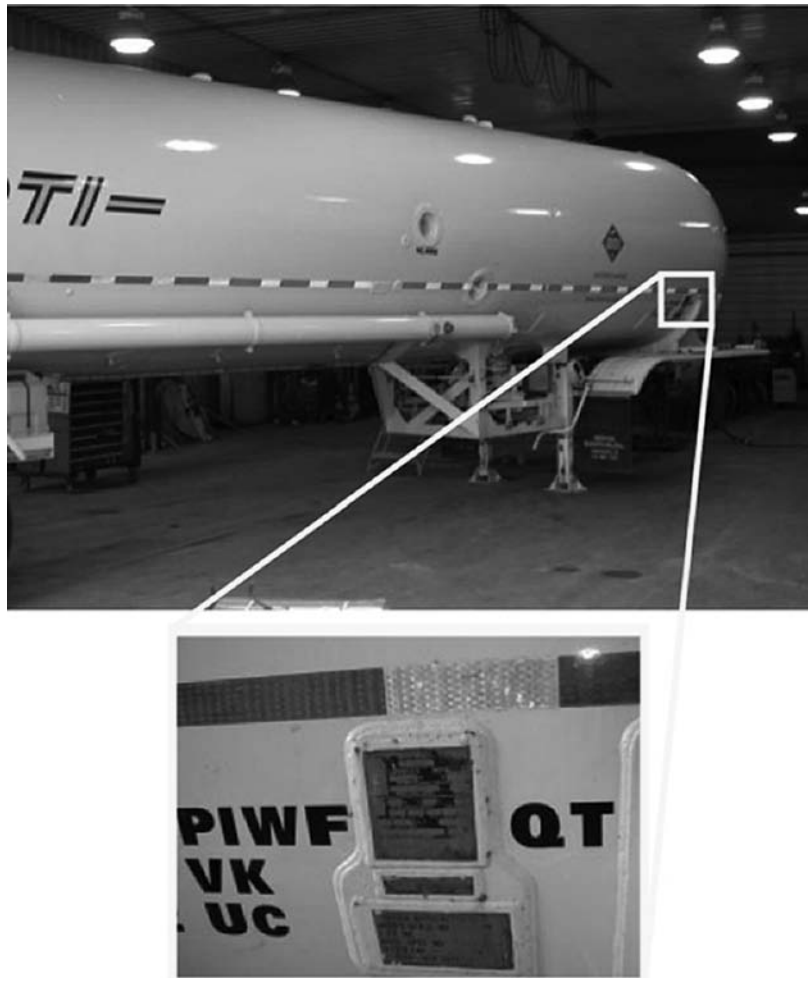

Fig. 49 Accident cargo tank with "QT" designation, which indicates quenched and tempered steel

© 2008 ASM International. All Rights Reserved.

sketch of the main landing gear assembly of a B-757 is shown in Fig. 52. The fracture surface, showing evidence of corrosion, is shown in Fig. 53.

Metallurgical analysis indicated that the fracture mode was due to SCC. Examination of the finish on the inner diameter showed that the plating on the inside diameter was thin or nonexistent, and that it did not receive the required shot peening. Because the truck beam was overhauled and the original plating was retained and worn during service, it was likely that the overhaul was inadequate or improper. This had the result of minimal cadmium protection on the inner diameter surface of the truck beam. Subsequent loss of the plating led to premature and severe corrosion in service and eventual fracture due to SCC.

Creep Rupture The effects of temperature on mechanical properties and material behavior are commonplace in everyday living. Examples include pipes bursting in the middle of winter, the expansion of a bridge in the middle of summer, and the sagging of a fireplace grate. Each of these examples is an indication that properties change with temperature. In addition, the previous discussion indicated that steels become more brittle as the temperature is decreased. There are many other effects of temperature that have been cited (Ref 63). Even the concept of elevated temperature is relative (Ref 64). What is considered hot for one material may be considered cold for another; for example, gallium has a melting point of 30 °C, while tungsten has a melting point of approximately 3400 °C.

Creep is the continuous deformation of a material as a function of time and temperature. This topic is treated very thoroughly in Ref 65. The creep of a material is shown in Fig. 54. It can be seen from the figure that creep in a material occurs in three stages:

- Stage I, where a rapid creep rate is seen at the onset of load application, then gradually decreases
- Stage II, where creep remains at a steady-state rate
- Stage III, where the creep rate shows an increasing rate until failure occurs

The behavior and creep rate are sensitive to the temperature to which the material is

Fig. 50 Through-the-wall crack on accident tanker

Fig. 51 Boeing 757-2008 truck beam failure occurring on Icelandic Air, aircraft registration TF-FIJ.

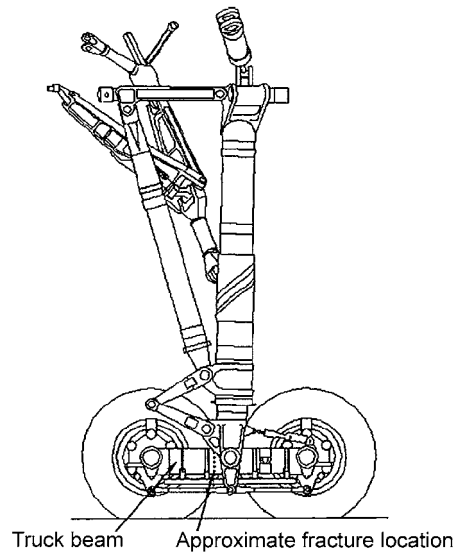

Fig. 52 Schematic of the assembly of a Boeing 757 main landing gear showing the location of fracture

© 2008 ASM International. All Rights Reserved.
Failure Analysis of Heat Treated Steel Component (#05113G) www.asminternational.org

exposed, the surrounding atmosphere, and the prior strain history. Andrade and Chalmers (Ref 66) were pioneers in the study of creep and proposed that creep followed the equation:

$$\varepsilon = \varepsilon_0(1 + \beta t^{1/3})e^{kt}$$

where β and k are material constants that can be evaluated by several different methods (Ref 67). A better fit for the creep of materials was proposed by Garofalo (Ref 68). He indicated that:

$$\varepsilon = \varepsilon_0 + \varepsilon_t(1 - e^{-n}) + \frac{d\varepsilon}{dt}t$$

where $d\varepsilon/dt$ is the steady-state creep rate, ε_0 is the strain on loading, n is the ratio of the transient creep rate to the transient creep strain, and ε_t is the transient creep strain.

Very early, it was recognized that fractures at elevated temperatures occurred along grain facets (Ref 69). In stage III creep, intergranular wedge cracks and cavities form. Wedge-shaped cracks and creep cavities usually initiate at or near grain-boundary triple points and propagate along grain boundaries normal to the applied tensile stress. Creep cavities form at higher temperatures and lower working stresses. These structural features are shown in Fig. 55.

Creep testing is usually performed for 1000 to 10,000 h with strains of up to 0.5%. Stress-rupture testing, or testing to failure, uses much higher loads and temperatures, and the test is usually terminated after 1000 h. In stress-rupture testing, the time to failure is measured at a constant stress and constant temperature. This test has gained acceptance for elevated-temperature testing of turbine blade materials in jet engines.

Using a tensile machine and high-temperature furnace, the strain is measured in creep testing by special extensometers suited for elevated temperatures. In stress-rupture testing, a simple apparatus such as a dial calipers is used, since only the overall strain at constant time and temperature is needed.

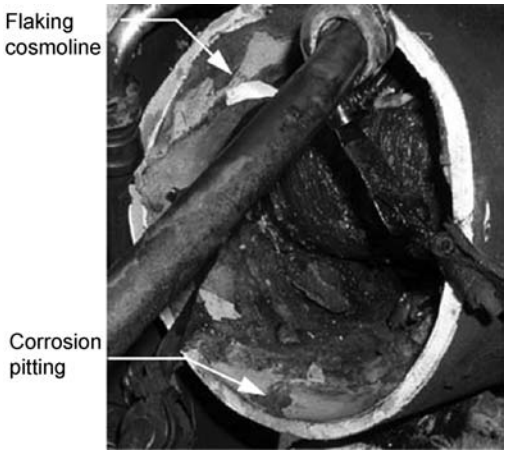

Fig. 53 Fracture surface of Boeing 757 main landing gear truck beam on Icelandic Air aircraft TF-FIJ

Fatigue

Parts are subject to varying stresses during service. These stresses are often in the form of repeated or cyclic loading. After enough applications of load or stress, the components fail at stresses significantly less than their yield strength. Fatigue is a measure of the decrease in resistance to repeated stresses.

Fatigue failures appear brittle, with no gross deformation. The fracture surface is usually normal to the main principal tensile stress. Fatigue failures are recognized by the appearance of a smooth, rubbed type of surface, generally in a semicircular pattern. The progress of the fracture (and crack propagation) is generally suggested by beach marks. This is illustrated in Fig. 56 and 57. The initiation site of fatigue failures is generally at a stress-concentration site or stress raiser. A typical fracture appearance is shown schematically in Fig. 58.

Three factors are necessary for fatigue to occur. First, the stress must be high enough that a crack is initiated. Second, the variation in the stress application must be large enough that the crack can propagate. Third, the number of stress applications must be sufficiently large that the crack can propagate a significant distance. The

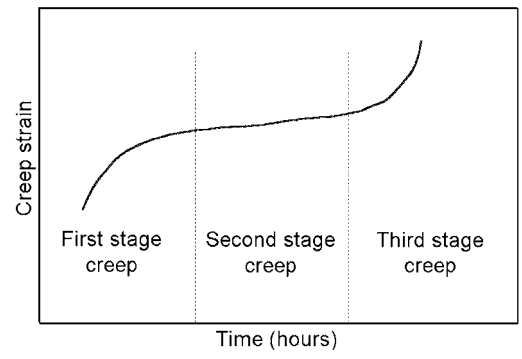

Fig. 54 Schematic representation of creep

© 2008 ASM International. All Rights Reserved.
Failure Analysis of Heat Treated Steel Component (#05113G) www.asminternational.org

fatigue life of a component is affected by a number of variables, including stress concentration, corrosion, temperature, microstructure, residual stresses, and combined stresses.

The structural features of fatigue failures are generally divided into four distinct areas (Ref 70):

- Crack initiation, the early development of fatigue damage
- Slip band crack growth, the early stages of crack propagation. This is often called stage I crack growth.
- Stable crack growth, which is usually normal to the applied tensile stress. This is called stage II crack growth.
- Unstable crack growth, with final failure from overload. This is called stage III crack growth.

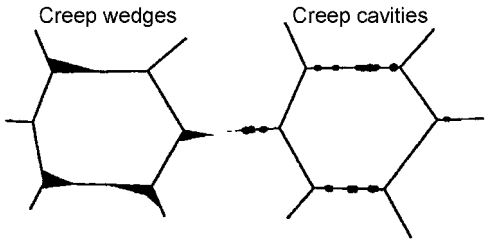

Fig. 55 Creep cavities and creep wedges forming at grain boundaries

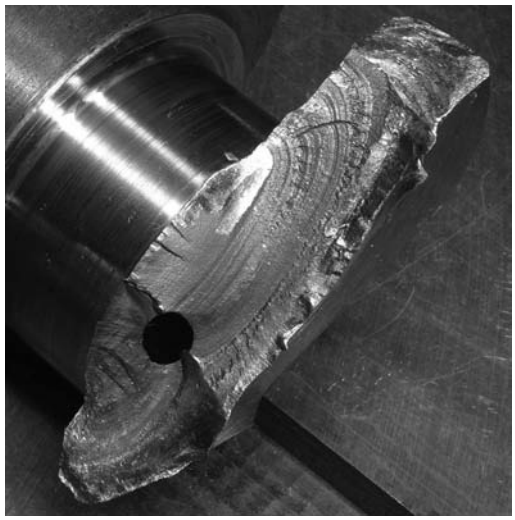

Fig. 56 Actual fatigue failure of a crankshaft showing characteristic beach marks. Fatigue initiated at the radius of the journal and exhibits classic bending fatigue.

Fatigue usually occurs at a free surface, with the initial features of stage I growth, fatigue cracks, being initiated at slip band extrusions and intrusions (Ref 71, 72). Cottrell and Hull (Ref 73) proposed a mechanism for the formation of these extrusions and intrusions (shown schematically in Fig. 59) that depends on the presence of slip, with slip systems at 45° angles to each other operating sequentially on loading and unloading. Wood (Ref 74) suggested that the formation of the intrusions and extrusions was the result of fine slip and buildup of notches (Fig. 60). The notch created on a microscopic scale would be the initiation site of stable fatigue crack growth.

In stage II, stable fatigue crack growth, striations (Fig. 61) often show the successive position of the crack front at each cycle of stress. Fatigue striations are usually detected using electron microscopy and are visual evidence that fatigue occurred. However, the absence of fatigue striations does not preclude the occurrence of fatigue.

Striations are formed by a plastic blunting process (Ref 75). At the end of the stage I crack tip, there exists sharp notches due to the presence of slip. These sharp notches cause stress to be concentrated at the crack tip. The application of a tensile load opens the crack along slip planes by plastic shearing, eventually blunting the crack tip. When the load is released, the slip direction reverses, and the crack tip is compressed and sharpened. This provides a sharp notch at the new crack tip where propagation

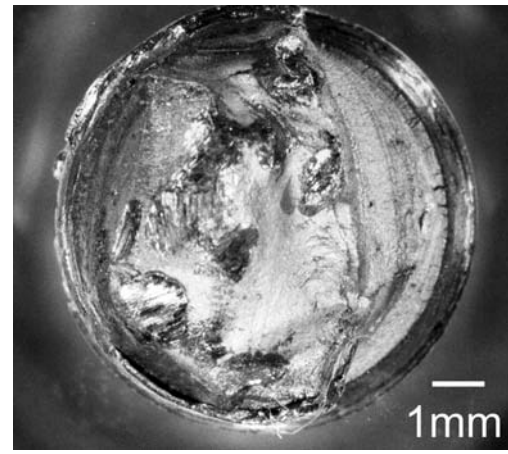

Fig. 57 Fatigue failure of a fastener, with initiation of fatigue occurring at the threads

© 2008 ASM International. All Rights Reserved.
Failure Analysis of Heat Treated Steel Component (#05113G)

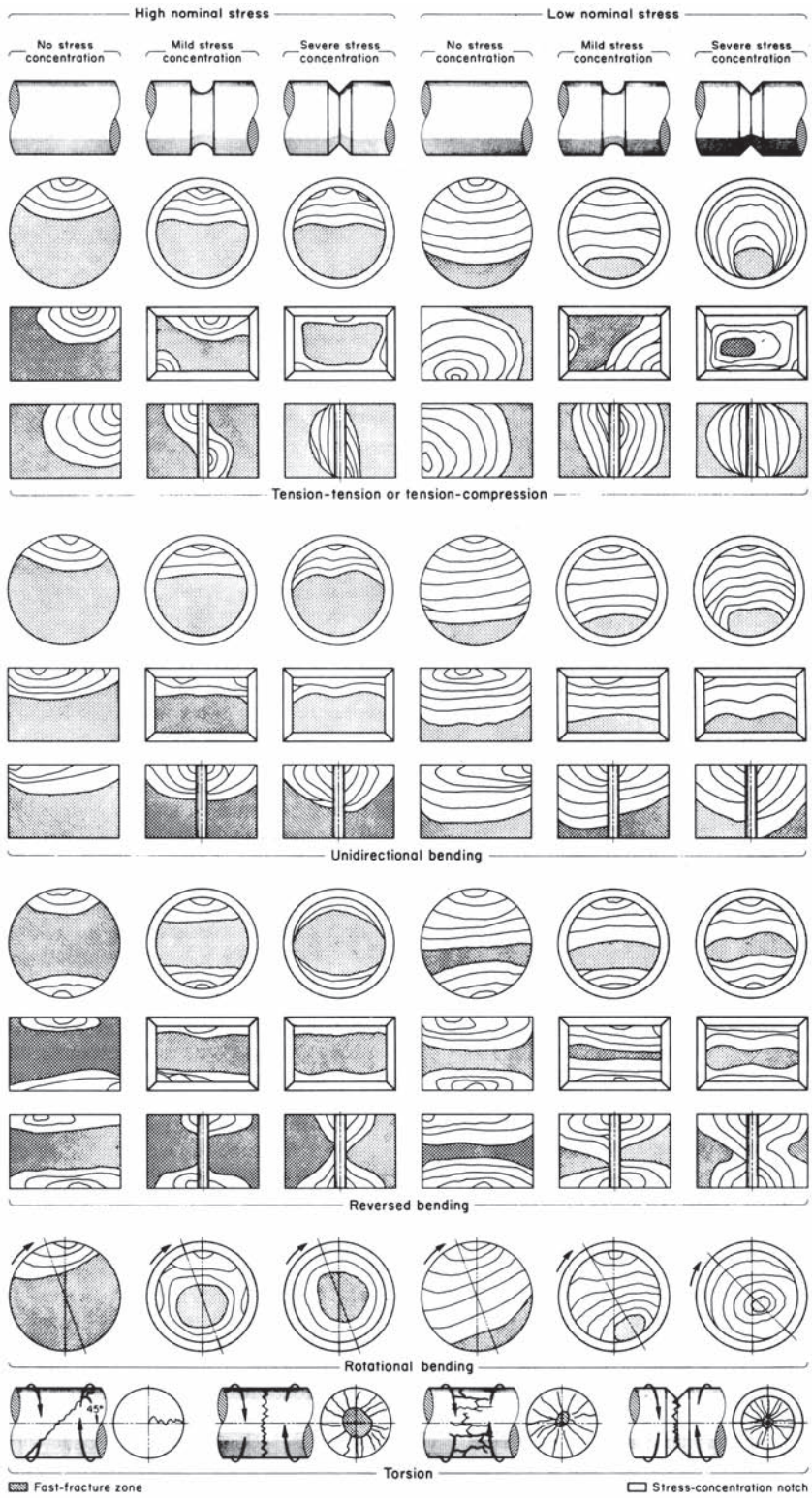

Fig. 58 Schematic illustration of simple fatigue failures

© 2008 ASM International. All Rights Reserved.

can occur. This is shown schematically in Fig. 62.

An alternative hypothesis on striation formation was presented by Forsyth and Ryder (Ref 76). In their model, the triaxial stress state at the crack tip forms a dimple ahead of the crack front. The material between the crack tip and the dimple contracts and eventually ruptures, forming a fatigue striation. This is shown schematically in Fig. 63.

In mild steel, well-defined striations are observed but not as well defined or as spectacular as in aluminum. This was first assumed to be due to the crystal lattice structure, since face-centered cubic austenitic steels show well-defined striations, and mild steels (base-structured) do not (Ref 77). Other alloys, such as titanium alloys, with a hexagonal close-packed crystal structure show very defined striations (Ref 78). However, aluminum alloys (body-centered cubic) show strongly defined striations (Ref 79). Therefore, attributing defined striations to crystal lattice alone was discounted as a viable theory.

Deformation and available slip systems were presumed to be more significant (Ref 80). However, this does not follow, because mild carbon steels are more ductile than austenitic steels. It is now generally accepted that fatigue striations form by the plastic blunting process.

It has also been found that the thicker the testpiece, the faster the crack propagation rate (Ref 81). It is likely that the propagation rates for thicker pieces are due to increased plane-strain conditions, with a small plastic zone at the crack tip. Since there is a greater stress gradient for a small plastic zone, a faster crack propagation rate may be expected. Also, in thicker panels there is a higher state of triaxial stress, which would also tend to increase crack growth rates.

Since fatigue failures usually begin at the surface, the surface condition is very important. Surface roughness is a primary factor influencing fatigue. Highly polished specimens exhibit the longest fatigue life, with increasingly rougher surfaces yielding decreased fatigue life. Rough lathe or coarse grinding reduces the fatigue strength by approximately 20% below polished specimens (Ref 82). Electropolished specimens have lower fatigue limits than mechanically polished specimens, by up to 25% (Ref 83). This reduction is due to the removal of surface compressive residual layers induced during mechanical finishing.

An example of a typical fatigue failure in an ASTM B7 low-alloy steel bolt grade is shown in Fig. 64 (Ref 9). Fracture initiation occurred along the threads with typical and pronounced beach marks (i.e., cyclic fracture propagation) and transgranular fracture mode.

An example of a manufacturing effect on fatigue is the following example of an arresting gear hook shank (Fig. 65) used to slow down aircraft when landing on aircraft carriers. In this example, the hook failed after 1361 simulated arrestments, which was below the lifetime of 2250 arrestments. The part is designed to last

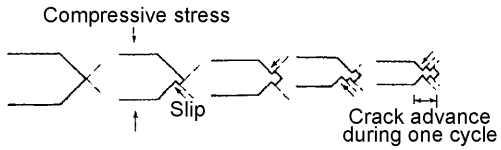

Fig. 59 Schematic representation of the mechanism of fatigue intrusions and extrusions

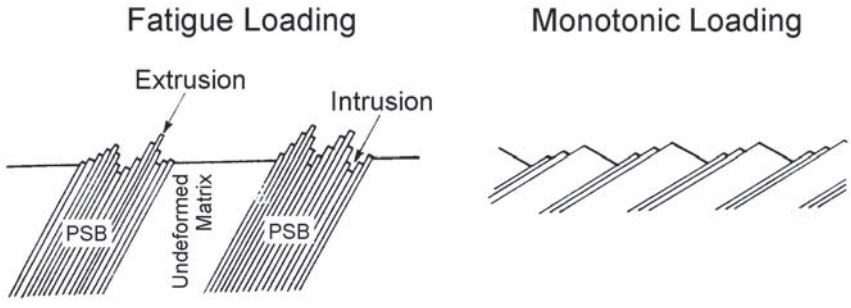

Fig. 60 Mechanism of intrusions and extrusions. PSB, persistent slip bands. Source: Ref 74

© 2008 ASM International. All Rights Reserved.
Failure Analysis of Heat Treated Steel Component (#05113G) www.asminternational.org

two lifetimes, or 4500 arrestments, without cracking (0.25 mm, or 0.010 in. detectible flaw). The arresting shank was fatigue tested in a fixture, with hydraulic cylinders providing loads at the vertical damper and hook-point cable groove. The maximum applied load was 90 mg (200,000 lb). A schematic of the arresting hook shank is shown in Fig. 65.

The arresting hook shank was fabricated from an AerMet 100 rotary forging. It is rough turned on a lathe on the outside, then gun drilled to create a pilot hole down the length of the forging. The outer surface is turned to the final diameter. The bore is then injection drilled to the final dimensions. A follower supported the injection drill. This is not a method that is commonly used for final machining operations. It is heat treated in vacuum to 1930 MPa (280 ksi) ultimate tensile strength. The part is inspected using dye-penetrant and magnetic particle nondestructive testing methods. The bore is visually inspected using a bore scope. This is a difficult inspection because of the long length and narrow bore.

Examination of the fracture surface showed that cracking initiated at the hook-point side, on the inner diameter, at a location approximately 26.5 cm (10.5 in.) aft of the uplock retainer. The fracture had characteristics of fatigue fracture, with multiple origins observed. Surface roughness measurements varied across the inner bore, from approximately 1 to 5 μm (40 to 180 μin.). The drawing requirement was 3 μm (125 μin.). Circumferential machining marks were found at the fracture origin (Fig. 66). SEM examination (Fig. 67) showed fatigue striations emanating away from the identified origin. Cracking was found to have initiated at circumferential machining marks. Machining marks were observed at 4.3 mm (0.17 in.) intervals. Many secondary cracks were observed at the machining marks. Fatigue was found to initiate subsurface to the inner bore, adjacent to the machining marks. A well-defined surface layer was observed. This layer had the appearance of mechanical working or damage. This observed layer followed the feeds and speeds of the injection drill. Metallography showed that the material was quenched and tempered martensite and was typical for this material heat treated to this hardness. At the

Fig. 61 Typical fatigue striations in 7075 aluminum

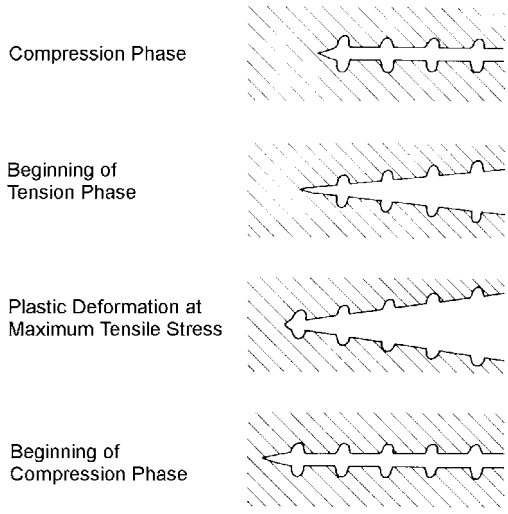

Fig. 62 Mechanism for fatigue striation formation

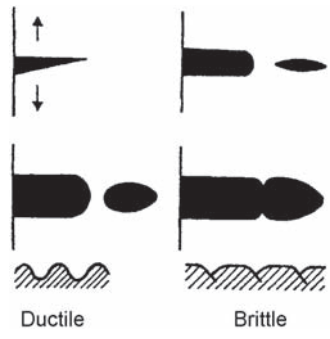

Fig. 63 Striation formation from ductile dimple formation ahead of a crack front

© 2008 ASM International. All Rights Reserved.
Failure Analysis of Heat Treated Steel Component (#05113G) www.asminternational.org

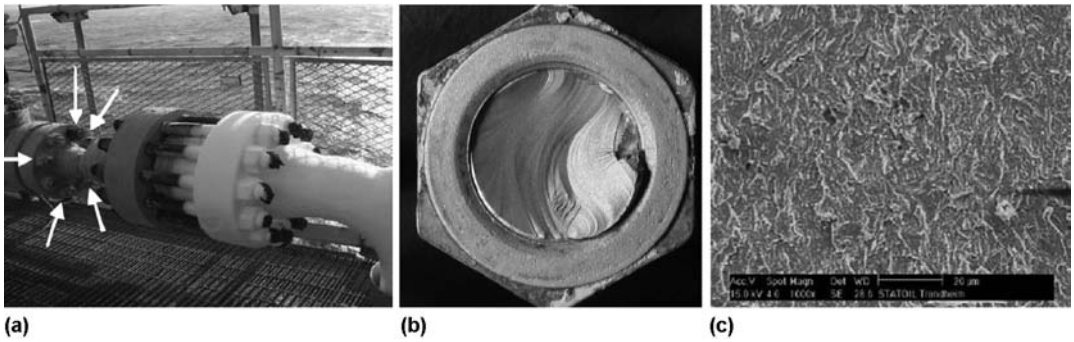

Fig. 64 ASTM B7 low-alloy steel bolt grade. Fracture initiated along threads, with typical and pronounced beach marks (i.e., cyclic fracture propagation) and transgranular fracture mode. (a) Location of bolts in pump coupling. (b) Beach marks showing asymmetrical bending with initiation at high stress-concentration factor at bolt threads. (c) Transgranular fracture morphology

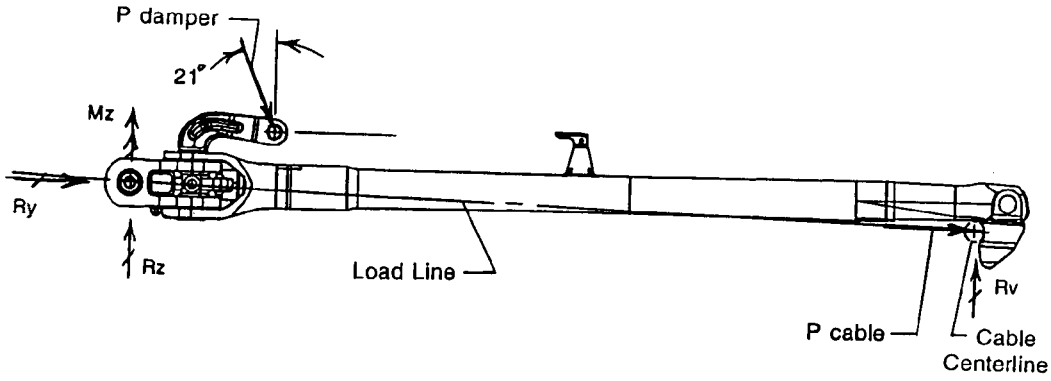

Fig. 65 Schematic of the failed arresting hook shank showing location of loads

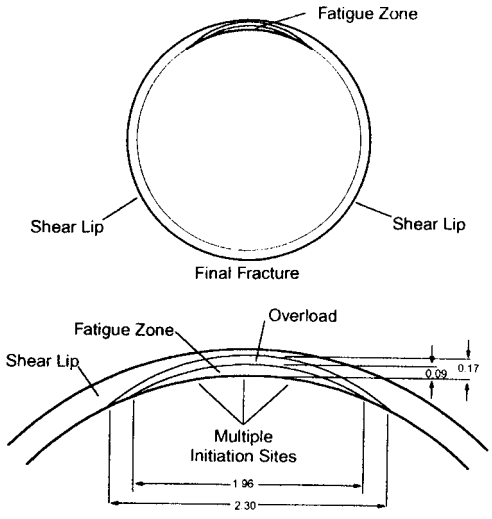

Fig. 66 Machining marks found on the inside of the bore, at the origin of cracking

origin, the presence of well-defined subsurface cracking was observed. This layer had the appearance of smeared metal and base metal pullout. Flat cracking, suggestive of fatigue cracking, was observed to emanate from the flaw (Fig. 68). The flaws were located at 4.3 mm (0.017 in.) intervals, identical to the feed rate of the injection drilling process.

During the injection drilling process, three cutters are used. Coolant is forced through a central hole to cool the cutting tools and to flush the chips. AerMet 100 tends to form long strands of material during machining and does not want to form chips. Hot chips can contact the freshly machined surface. These chips or long strands are under pressure at the cutter or follower and can be forced onto the newly machined surface by the follower. If the temperature and pressures are high enough, solid-state welding of the chips and bore surface can occur. As the cutter boring bar moves, pullout can occur. The

© 2008 ASM International. All Rights Reserved.
Failure Analysis of Heat Treated Steel Component (#05113G) www.asminternational.org

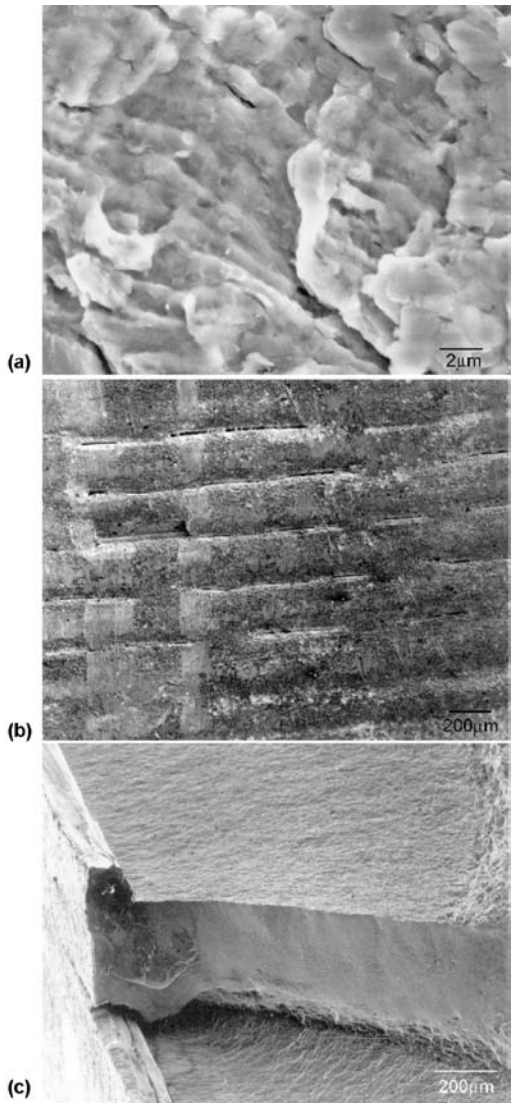

Fig. 67 SEM examination of the fracture surface. (a) Fatigue striations emanating from the fracture origin. (b) Machining marks found on the surface of the inner bore. (c) Well-defined layer showing fatigue emanating from the damaged material at the surface of the inner bore

examined flaws matched the machining feeds and speeds.

The arresting hook failed by fatigue, initiating at flaws created during the final machining process. The defect morphology suggested localized solid-state welding and pullout from chip contact with the freshly machined surface. The surface roughness and finish of the inner bore did not meet drawing requirements.

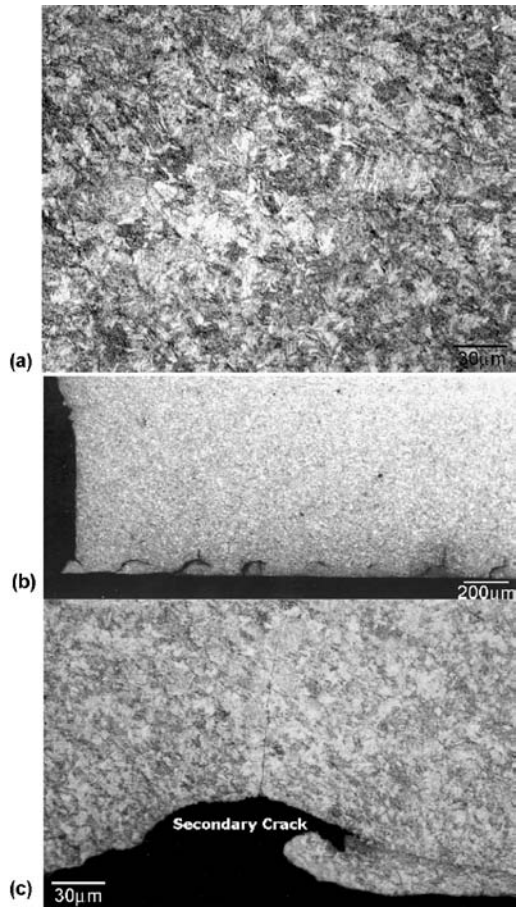

Fig. 68 Metallography of the arresting hook shank. (a) Typical quenched and tempered martensite found. This is typical for the hardness of the arresting hook shank. (b) Pulled material at 4.3 mm (0.17 in.) intervals along the inner bore of the arresting hook shank. Origin is to the left. (c) Secondary cracking observed at the location of pulled material

Summary

In this short overview of the possible mechanisms of failure for steels, the following were discussed:

- Techniques for examining fractures
- Ductile and brittle failures
- Intergranular failure mechanisms
- Fatigue

The previous discussion has shown that it is important to look at not only the fracture surface but at all the factors (manufacturing history, service conditions, and loading). All the tools available to the metallurgist should be used—these include photography, fractography, and

© 2008 ASM International. All Rights Reserved.
Failure Analysis of Heat Treated Steel Component (#05113G) www.asminternational.org

metallography—to understand the sources and root cause of failure.

REFERENCES

1. Hippocrates, *Epidemics,* Book I, Section XI
2. D.S. MacKenzie, G. Chen, M. Barker, C. Ramsay, J. Alderson, L. Dharani, and J. Yu, Forensic Investigation of Failed Mast Arms of Traffic Signal Supported Structures, *Transport. Res. Record, Des. Struc. 2002,* 2002, p 9–16
3. "Loss of Control and Impact with Pacific Ocean Alaska Airlines Flight 261 McDonnell Douglas MD-83, N963AS about 2.7 Miles North of Anacapa Island, California, January 31, 2000," NTSB/AAR-02/01, National Transportation Safety Board, Adopted Dec 30, 2002, Notation 7263E
4. "Uncontained Engine Failure/Fire Valujet Airlines Flight 597 Douglas DC-9-32, N908VJ, Atlanta, Georgia, June 8, 1995," NTSB/AAR-96/03, National Transportation Safety Board, Adopted July 30, 1996, Notation 6579A
5. W.M. Garrison and N.R. Moody, *J. Phys. Chem. Solids,* Vol 48, 1987 p 1035
6. J.F. Knott, Advances in Fracture Research, *Proc. Seventh International Conference on Fracture* (Oxford, U.K.) 1989, p 125
7. J.F. Knott, *Fracture 1977,* Vol 1, *Proc. Fourth International Conference on Fracture,* June 1977 (Waterloo Canada), p 61
8. H.G. Wilsforf, *Mater. Sci. Eng.,* Vol 59, 1983, p 1
9. B. Bøgner, G. Rørvik, and L. Marken, Bolt Failures—Case Histories from the Norwegian Petroleum Industry, *Microsc. Microanal.,* Vol 11 (Suppl. 2), 2005, p 1604–1605
10. T.L. Anderson, *Fracture Mechanics,* CRC Press, New York, 1995
11. C. Ruggieri, Numerical Investigation of Constraint Effects on Ductile Fracture in Tensile Specimens, *J. Braz. Soc. Mech. Sci. Eng.,* Vol 26 (No. 2), 2004
12. "Standard Test Methods for Determining the Inclusion Content of Steel," E45–05, ASTM International
13. "Premium Aircraft-Quality Steel Cleanliness: Magnetic Particle Inspection Procedure," AMS 2300
14. "Aircraft-Quality Steel Cleanliness: Magnetic Particle Inspection Procedure," AMS 2301
15. "Aircraft-Quality Steel Cleanliness: Martensitic Corrosion-Resistant Steels Magnetic Particle Inspection Procedure," AMS 2303
16. "Special Aircraft-Quality Steel Cleanliness: Magnetic Particle Inspection Procedure," AMS 2304
17. R. Kiessling and N. Lange, *Non-Metallic Inclusions in Steel, Part I–IV,* Iron and Steel Institute, London, 1978
18. S. Maropoulos and N. Ridley, Inclusions and Fracture Characteristics of HSLA Steel Forgings, *Mater. Sci. Eng. A,* Vol 384 (No. 1–2), Oct 25, 2004, p 64–69
19. "Railway Investigation Report, Derailment and Collision Canadian National Train No. U-783-21-30 and Train No. M-306-31-30 Mile 50.84, Saint-Hyacinthe Subdivision Mont-Saint-Hilaire, Quebec, December 30 1999," Report R99H0010, Transportation Safety Board of Canada
20. M.L. Williams, STP 158, ASTM, 1954, p 11–44
21. M.E. Shank, STP 158, ASTM, 1954, p 45–110
22. *Fractography,* Vol 12, *Metals Handbook,* 9th ed., ASM International, 1987
23. J. McCall and P. French, *Metallography in Failure Analysis,* Plenum, New York, 1978, p 6
24. "Standard Test Methods for Notched Bar Impact Testing of Metallic Methods," E23–88, American Society for Testing and Materials
25. "Standard Test Method for Plane Strain Fracture Toughness, K_{Ic}, of Metallic Materials," E399–74, American Society for Testing and Materials
26. "Standard Test Method for Conducting Drop-Weight Test to Determine Nil-Ductility Transition Temperature of Ferritic Steels," E208–95A, American Society for Testing and Materials, 1983
27. "Standard Test Method for Dynamic Tear Testing of Metallic Materials," E604–83, American Society for Testing and Materials, 1983
28. J.M. Kraft, A.M. Sullivan, and R.W. Boyle, *Proc. Symp. Crack Propagation,* Cranfield, U.K., 1961
29. W.F. Brown and J.E. Strawley, *STP 381,* American Society for Testing and Materials, 1965, p 133
30. A.S. Tetelman and A.J. McEvily, *Fracture of Structural Materials,* Wiley, New York, 1967

© 2008 ASM International. All Rights Reserved.
Failure Analysis of Heat Treated Steel Component (#05113G) www.asminternational.org

31. J.F. Knott, *Fundamentals of Fracture Mechanics,* Wiley, New York, 1973
32. A.H. Cottrell, *Proc. R. Soc. A,* Vol 276 (No. 1), 1963
33. A.H. Knott, *Mater. Sci. Eng.,* Vol 7 (No. 1), 1971
34. J.S. Colton, Class notes, "Great Boston Molasses Disaster, Jan 15, 1919," ME6222 Manufacturing Processes and Systems, Georgia Institute of Technology
35. G. Krauss, *Steels: Heat Treatment and Processing Principles,* ASM International, 1990, p 231, 237
36. G. Thomas, Retained Austenite and Tempered Martensite Embrittlement, *Metall. Trans. A,* Vol 10, 1979, p 1643–1651
37. S. Banerji, C. McMahon, and H. Feng, Intergranular Fracture in 4340-Type Steels: Effects of Impurities and Hydrogen, *Metall. Trans. A,* Vol 9, 1978, p 237–247
38. D. Kalderon, Steam Turbine Failure at Hinkley Point 'A', *Proc. Inst. Mech. Eng.,* Vol 186, 1972, p 341–377
39. L.D. Kramer and D. Randolph, Analysis of TVA Gallatin No. 2 Rotor Burst: Part 1—Metallurgical Considerations, *Proc. 1976 ASME-MPC Symposium on Creep-Fatigue Interaction,* p 1–24
40. H.K.D.H. Bhadeshia, High Performance Bainitic Steels, *Mater. Sci. Forum,* Vol 500, 2005, p 63–74
41. I. Olefjord, Temper Embrittlement, Review 231, *Int. Met. Rev.,* Vol 23, 1978, p 149–163
42. B. Woodfine, Temper Brittleness, A Critical Review of the Literature, *JISI,* Vol 173, 1953, p 229–240
43. F. Carr, M. Golman, L. Jaffee, and D. Buffum, Isothermal Temper Embrittlement of SAE 3140 Steel, *Trans. TMS-AIME,* Vol 197, 1953, p 998
44. Liquid Metal Embrittlement, *Failure Analysis and Prevention,* Vol 10, *Metals Handbook,* 8th Ed., American Society for Metals, 1975, p 228–229
45. P. Fernandez, R. Clegg, and D. Jones, Failure by Liquid Metal Induced Embrittlement, *Eng. Fail. Anal.,* Vol 1 (No. 1), 1994, p 51–63
46. G. Vilganlte, G. Troiano, and C. Mossey, "Liquid Metal Embrittlement of ASTM A723 Gun Steel by Indium and Gallium," ARCCB-TR-99011, Army Research, Development and Development Center, Benet Laboratories, Watervliet Arsenal, June 1999
47. NTSB CHI97IA117, National Transportation Safety Board, adopted June 28, 1998
48. NTSB Safety Recommendation, in memo to J. Garvy, Administrator A-97-83, FAA, Aug 29, 1997
49. S.F. Carter, Effect of Melting Practice on Hydrogen, *J. Met. (AIME),* Vol 188, Jan 1950, p 30–40 and *J. Met. (AIME),* Vol 188, Feb 1950, p 245–255
50. F.B. Foley, Flakes and Cooling Cracks in Forgings, *Met. Alloys,* Vol 12, 1940, p 442–445
51. F.J. Shortsleeve and A.R. Troiano, "A Literature Survey on the Mechanism of Flake Formation," Interim Technical Report 1, Contract DA 33-019-ORD-897
52. C.A. Edwards, Pickling or the Action of Acid Solution on Mild Steel and the Diffusion of Hydrogen Through the Metal, *J. Iron Steel Inst.,* Vol 110, 1924, p 9–60
53. C.A. Zapffe and M.E. Haslem, Acid Composition, Concentration Temperature and Pickling Time as Factors in the Hydrogen Embrittlement of Mild Steel and Stainless Steel Wire, *Trans. ASM,* Vol 39, 1947, p 213–236
54. J.R. Gustafson, Some of the Effects of Cadmium, Zinc, and Tin Plating on Springs, *Proc. ASTM,* Vol 47, 1947, p 782
55. K.B. Valentine, Stress Cracking of Electroplated Lockwashers, *Trans. ASM,* Vol 38, 1947, p 488–504
56. C.A. Zapffe and M.E. Haslem, Measurement of Embrittlement during Chromium and Cadmium Electroplating and the Nature of Recovery of Plated Articles, *Trans. ASM,* Vol 39, 1947, p 241–258
57. G. Nagu and T. Namboodhiri, Effect of Heat Treatments on the Hydrogen Embrittlement Susceptibility of API X-65 Grade Line-Pipe Steel, *Bull. Mater. Sci.,* Vol 26 (No. 4), June 2003, p 435–439
58. A. Thompson and I. Berstein, Ed., *Effect of Hydrogen on Behavior of Materials,* TMS-AIME, 1976
59. H. Johnson, J. Morlet, and A. Troiano, Hydrogen Crack Initiation and Delayed Failure in Steel, *Trans. TMS-AIME,* Vol 212, 1958, p 528–536
60. "Release of Hazardous Materials from Cargo Tank in Middletown, Ohio, on August 22, 2003," Accident DCA03MZ002, NTSB

© 2008 ASM International. All Rights Reserved.
Failure Analysis of Heat Treated Steel Component (#05113G) www.asminternational.org

Hazardous Materials Accident Brief, Adopted July 22, 2004
61. A.W. Loginow, Stress-Corrosion Cracking of Steel in Liquefied Ammonia Service, *Bull., Natl. Board Boiler Pressure Vessel Insp.,* Vol 45 (No. 6), Oct 1988
62. "Report by the Danish Accident Investigation Board into the Incident to Boeing 757, TF-FIJ at Kastrup Airport, Denmark on June 28, 2001," M-04001/AIG-09, Danish Accident Review Board
63. J.E. Dorn, Ed., *Mechanical Behavior of Materials at Elevated Temperature,* McGraw-Hill, New York, 1961
64. R.W. Guard, *Prod. Eng.,* Vol 27 (No. 10), 1956, p 160–174
65. I. Finnie and W.R. Heller, *Creep of Engineering Materials,* McGraw-Hill, New York, 1959
66. E.N. da C. Andrade and B. Chalmers, *Proc. R. Soc. (London) A,* Vol 138, 1932, p 348
67. J.B. Conway, *Trans. Metall. Soc. AIME,* Vol 223, 1965, p 2018
68. F. Garofalo, *Properties of Crystalline Solids,* STP 283, ASTM, 1965
69. W. Rosenhahn and D. Ewen, *J. Inst. Met.,* Vol 10, 1913, p 119
70. W.J. Plumbridge and D.A. Ryder, *Metall. Rev.,* Vol 14, 1969, p 136
71. P.J. Forsyth and C.A. Stubbington, *J. Inst. Met.,* Vol 83, 1955, p 395
72. W.A. Wood, *Some Basic Studies of Fatigue in Metals,* Wiley, New York, 1959
73. A.H. Cottrel and D. Hull, *Proc. R. Soc. (London) A,* Vol 242A, 1953, p 211
74. W.A. Wood, *Bull. Inst. Met.,* Vol 3, 1955, p 5
75. C. Laird, "Fatigue Crack Propagation," in STP 415, American Society for Testing and Materials, 1967, p 136
76. P.J. Forsyth and D.A. Ryder, *Metallurgica,* Vol 63, 1961, p 117
77. G. Jacoby, *Current Aeronautical Fatigue Problems,* J. Schijve, Ed., Pergamon, New York, 1965, p 78
78. W.R.Warke and J.M. McCall, "*Fractography Using the Electron Microscope,*" ASM Technical Report We-2-65, American Society for Metals, 1965
79. G. Jacoby, Fractographic Methods, *Exp. Mech.,* 1965, p 65
80. P.J. Forsyth, A Two Stage Process of Fatigue Crack Growth, *Symp. Crack Propagation,* Vol 2, Cranfield, U.K., 1961, p 76
81. D. Broek and J. Schijve, "*The Influence of Sheet Thickness in the Fatigue Crack Propagation in* 2024-T3 *Alclad Sheet Material,*" NLR Technical Report M2129, Amsterdam, 1963
82. N.E. Frost, K.J. Marsh, and L.D. Pook, *Metal Fatigue,* Oxford University Press, London, 1974
83. T.T. Oberg and E.J. Wad, Technical Note Report 56-289, Wright Air Development Department, 1956

ASM International is the society for materials engineers and scientists, a worldwide network dedicated to advancing industry, technology, and applications of metals and materials.

ASM International, Materials Park, Ohio, USA
www.asminternational.org

This publication is copyright © ASM International®. All rights reserved.

Publication title	Product code
Failure Analysis of Heat Treated Steel Components	**05113G**

To order products from ASM International:

Online Visit www.asminternational.org/bookstore

Telephone 1-800-336-5152 (US) or 1-440-338-5151 (Outside US)

Fax 1-440-338-4634

Mail Customer Service, ASM International
9639 Kinsman Rd, Materials Park, Ohio 44073-0002, USA

Email CustomerService@asminternational.org

In Europe American Technical Publishers Ltd.
27-29 Knowl Piece, Wilbury Way, Hitchin Hertfordshire SG4 0SX, United Kingdom
Telephone: 01462 437933 (account holders), 01462 431525 (credit card)
www.ameritech.co.uk

In Japan Neutrino Inc.
Takahashi Bldg., 44-3 Fuda 1-chome, Chofu-Shi, Tokyo 182 Japan
Telephone: 81 (0) 424 84 5550

Terms of Use. This publication is being made available in PDF format as a benefit to members and customers of ASM International. You may download and print a copy of this publication for your personal use only. Other use and distribution is prohibited without the express written permission of ASM International.

No warranties, express or implied, including, without limitation, warranties of merchantability or fitness for a particular purpose, are given in connection with this publication. Although this information is believed to be accurate by ASM, ASM cannot guarantee that favorable results will be obtained from the use of this publication alone. This publication is intended for use by persons having technical skill, at their sole discretion and risk. Since the conditions of product or material use are outside of ASM's control, ASM assumes no liability or obligation in connection with any use of this information. As with any material, evaluation of the material under end-use conditions prior to specification is essential. Therefore, specific testing under actual conditions is recommended.

Nothing contained in this publication shall be construed as a grant of any right of manufacture, sale, use, or reproduction, in connection with any method, process, apparatus, product, composition, or system, whether or not covered by letters patent, copyright, or trademark, and nothing contained in this publication shall be construed as a defense against any alleged infringement of letters patent, copyright, or trademark, or as a defense against liability for such infringement.